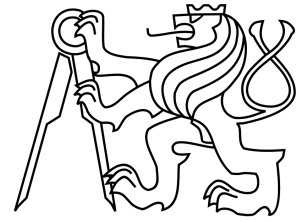CZECH TECHNICAL UNIVERSITY IN PRAGUE

Faculty of Civil Engineering
Department of Mechanics

Trabecular structure as the basis for modern implants

Trabekularní struktura jako základ moderních implantátů

Master thesis

Author: Bc. Petr Vakrčka

Supervisor: Ing. Aleš Jíra, Ph.D.

Master degree study program: Civil engineering

Field of study: Structural and Transportation Engineering

Prague, 2019

ČESKÉ VYSOKÉ UČENÍ TECHNICKÉ V PRAZE

Fakulta stavební
Thákurova 7, 166 29 Praha 6

ZADÁNÍ DIPLOMOVÉ PRÁCE

I. OSOBNÍ A STUDIJNÍ ÚDAJE

Příjmení: Vakrčka   Jméno: Petr   Osobní číslo: 423551

Zadávající katedra: Katedra mechaniky - k132

Studijní program: Stavební inženýrství

Studijní obor: Konstrukce a dopravní stavby

II. ÚDAJE K DIPLOMOVÉ PRÁCI

Název diplomové práce: Trabekulární struktura jako základ moderních implantátů

Název diplomové práce anglicky: Trabecular structure as the basis for modern implants

Pokyny pro vypracování:

Popis anatomie, histologie a základních materiálových parametrů částí lidského skeletu.
Popis soudobých technologií výroby nitrokostních částí implantátů a jejich povrchových úprav.
Možnosti využití aditivních technologií k výrobě trabekulárních struktur.
Návrh geometrie struktur, testovacích těles a jejich destruktivní mechanické hodnocení.
Vytvoření numerického modelu vybrané struktury a jeho porovnání jeho chování v MKP s experimentem.
Aplikace struktury na nitrokostní část implantátu.

Seznam doporučené literatury:
Odborné články a publikace dostupné v databázích WoS a SCOPUS, uživatelské manuály k systémům ANSYS,
případně SIFEL

Jméno vedoucího diplomové práce: Ing. Aleš Jíra, Ph.D.

Datum zadání diplomové práce: 27.2.2019   Termín odevzdání diplomové práce: 19.5.2019
Údaj uveďte v souladu s datem v časovém plánu příslušného ak. roku

Podpis vedoucího práce   Podpis vedoucího katedry

III. PŘEVZETÍ ZADÁNÍ

Beru na vědomí, že jsem povinen vypracovat diplomovou práci samostatně, bez cizí pomoci, s výjimkou poskytnutých konzultací. Seznam použité literatury, jiných pramenů a jmen konzultantů je nutné uvést v diplomové práci a při citování postupovat v souladu s metodickou příručkou ČVUT „Jak psát vysokoškolské závěrečné práce" a metodickým pokynem ČVUT „O dodržování etických principů při přípravě vysokoškolských závěrečných prací".

4.3.2019

Datum převzetí zadání   Podpis studenta(ky)

As the author of this master thesis, I declare no conflict of interest. I claim to have written this thesis solely myself, provided with professional consultations from my supervisor Ing. Aleš Jíra Ph.D.

I Also declare that all literature and materials used in the writing of this master thesis are appropriately cited in the Reference chapter

In Prague, May 19, 2019   Petr Vakrčka

Název práce: Trabekulární struktura jako základ moderních implantátů

Autor: Bc. Petr Vakrčka

Katedra (ústav): Katedra mechaniky

Vedoucí diplomové práce: Ing. Aleš Jíra, Ph.D.

E-mail vedoucího: jira@fsv.cvut.cz

Abstrakt Práce se zaobíra využití trabekulárních struktur jako náhrada za povrchovou úpravu stávajících implantátů. Toto je umožněno prostřednictvím aditivní výroby, která nám dovoluje komerční produkci různorodých tvarů s proměnnou porozitou. Pro bližší seznámení s problematikou se práce zpočátku věnuje popisu anatomie a histologie lidského těla, aditivní výrobou a přehledem druhů implantátů, které jsou běžné v oblasti implantologie.

Dále následuje výběr nejefektivnějšího uspořádání porézní struktury z hlediska výrobního a biokompatibilního. Na základě vybrané struktury byly vyrobeny vzorky z titaničité slitiny Ti6Al4V, které podstoupily mechanické zkoušky v tlaku. Následně byl vytvořen numerický model, který byl metodou curve-fitting upraven, aby odpovídal mechanickým testům.

Práce obsahuje také porovnání trámčitých a stěnových pórovitých struktur se zaměřením na mechanické vlastnosti a množství výrobních vad. V závěru práce se navrhuji možnosti dalšího pokračování výzkumu problematiky.

Klíčová slova: implantát, trabekulární kost, gyroid, titaničitá slitina, aditivní výroba, numerický model

Title: Trabecular structure as the basis for modern implants

Author: Bc. Petr Vakrčka

Department: Department of mechanics

Supervisor: Ing. Aleš Jíra, Ph.D.

Supervisor's e-mail address: jira@fsv.cvut.cz

Abstract In the present work, I study the application of trabecular structures as a substitution for surface modifications of the contemporary implant by using additive manufacturing. The additive manufacturing allows us to produce various shapes with variable porosity commercially. As an introduction to problematic, the work begins with the anatomical and histological description of the human body, the process of additive manufacturing, an overview of implants that are used in the field implantology daily.

Next part of the thesis focus on the selection of the most effective morphology of porous structure in term of production and biocompatibility. Based on selected morphology, there were produced specimens from titanium alloys Ti6Al4V which underwent mechanical compression testing. Afterward, the numerical models were created and optimized by the curve-fitting method to correspond with the results of mechanical testing.

The presented paper also contains a comparison of strut-based and plane-based porous structures in terms of mechanical properties and also the number of fractures during production. The end takes a look at the possibility of future research.

Keywords: implant, trabecular bone, gyroid, titanium alloy, additive manufacturing, numerical model

CONTENTS

FIRST

INTRODUCTION

Thanks to modern medicine and advancing technological progress, people across the world are living longer than ever before. The technology has become vital to give the patient the best care as possible. Many patients in the past had to suffer because there was not any technology to support them. Nowadays, people do not have to suffer anymore because technology is on their side. Since engineers started improving medical care, new medical devices have been created, modern software has been adapted, and technology has increase hospitality for every patient. For example, laparoscopic surgeries have become the norm for many operations. They are minimally invasive, cause less pain, and short the recovery time. The next great achievement in the field of medicine in recent years is Targeted cancer therapy, which can interfere with the spread of cancer by blocking cells involved in tumor growth. Worth mentioning is the Czech plastic surgeon Bohdan Pomahač who performed the first full face transplant, and the list of recent achievements in the medical field goes on. The presented thesis is, however, focusing on the particular field of medicine, which is implantology.

Figure 1.1: Various application of trabecular structures in nature [1]. In the left we can see the structure of leaf. In the right, we can see trabecular bone morphology [2]

The evolution made the body as perfect as possible. That is why the attempt to adequate reconstruction has been close to pursuing the "holy grail." For this reason, the majority of attempts have been unsuccessful. The human effort has made massive progress since the first primitive implants from ancient Egypt until custom-made implants made from titanium alloys by the 3D printer. At first, the implants meant to be for privileged ones. Nowadays, implants have become an available device for the ordinary people.

Even now, there are many challenges for engineers. The crucial is the implant contact area with the living tissue. The presented thesis sets a goal to knock down the problem by using a different approach than most of the current implants. In general, the contemporary implants have various surface modifications. Thanks to additive manufacturing, we can print almost every shape in a 3D printer. It allows us to substitute the surface modification by a suitable structure which can minimalize the risk of implant loss. The trabecular structure, which can be seen all around ourselves is the answer to this complicated question. We can see the application of the structure in figure 1.1.

SECOND

BONE ANATOMY

Bones are loaded permanently by an interaction of muscles connected to the bone. The bone structure is optimized to withstand the constant mechanical loading. As we grow older, our bone tissue decreases in mass, stiffness, and strength. In time, bone instability can occur. This term refers to the stage when the bone mass decrease to the critical level and the danger of fracture is increasing.

2.1 Description of the cortical bone

The main characteristic of this bone type is high density, hardness, and stiffness. It forms approximately 80 weight percent of the skeleton. The essential function of this bone type is structural and load-bearing; that is the reason why it prevails in the long bones of the skeleton. According to the microscopic structure, we can divide the cortical bone into fibrous bone and lamellae. Due to human evolution, the bone adjusts to the main stress of its typical loading with the need for minimal mass. As you can see in the figure 2.1 the current architecture of the lower jaw depends on the lines of the main stresses. [3]
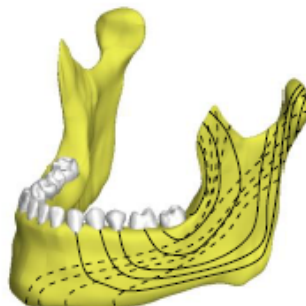

Figure 2.1: Tension and compression lines of the mandibular condylar (bone of the lower jaw) [4]

2.2 Description of the trabecular bone

Trabecular bone tissue is a spongy internal bone. Architecture is comprised of a seemingly stochastic assembly of rods and plates. It is an inner part of the cortical bone. Substantial evidence supports the hypothesis that trabecular bone optimizes its structure to support and transfer loads within bones and across joints. [4]. In conclusion, we can state the trabecular bone has low mechanical properties, lower density, higher porosity, and a higher concentration of blood vessels compared to its counterpart cortical bone. The porosity of trabecular bone is between 78% and 95%, whereas cortical bone is in the range of 5-10%. [5]
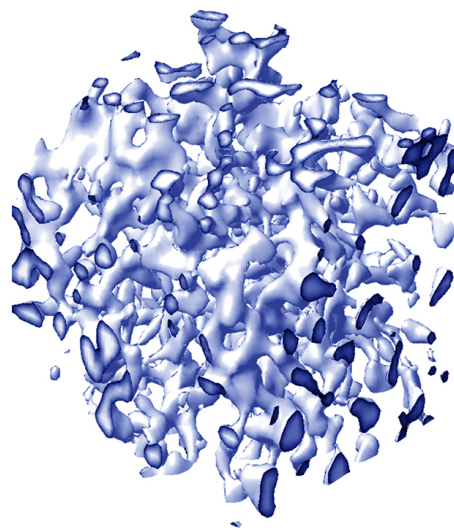
Figure 2.2: Trabecular bone [6]

2.3 Remodeling of the bone tissue

There can be found local differences in the bone due to remodeling. It is the reaction to the change of mechanical stress in time. Wolff's law describes this process. Julius Wolf (1836-1902) studied the connection between the mass of bones and the loading, which the system underwent. It states that every change in the function of stress in a bone is followed by specific, certain changes in internal architecture and external confirmation. Furthermore, the law defines that 25% of trabecular bone and 3% of cortical bone are restored in one year. [7]

The whole process of remodeling takes 200 days to finish for most of the population from 19 to 60 years of age. The method of remodeling is divided into four stages: [7]

1. Activation – signals from osteocytes activate osteoclasts

2. Resorption – multicellular osteoclasts initiate resorption of the old bone

3. Formation of the new bone and mineralization - the release of the growth factors activate osteoblasts that provide mineralization of the bone and determinate bone mineral content. Increasing, decreasing or maintaining bone mass depend on the change of stress in the bone.

4. Quiescence – it is a stage of stagnation of the architecture of the bone.
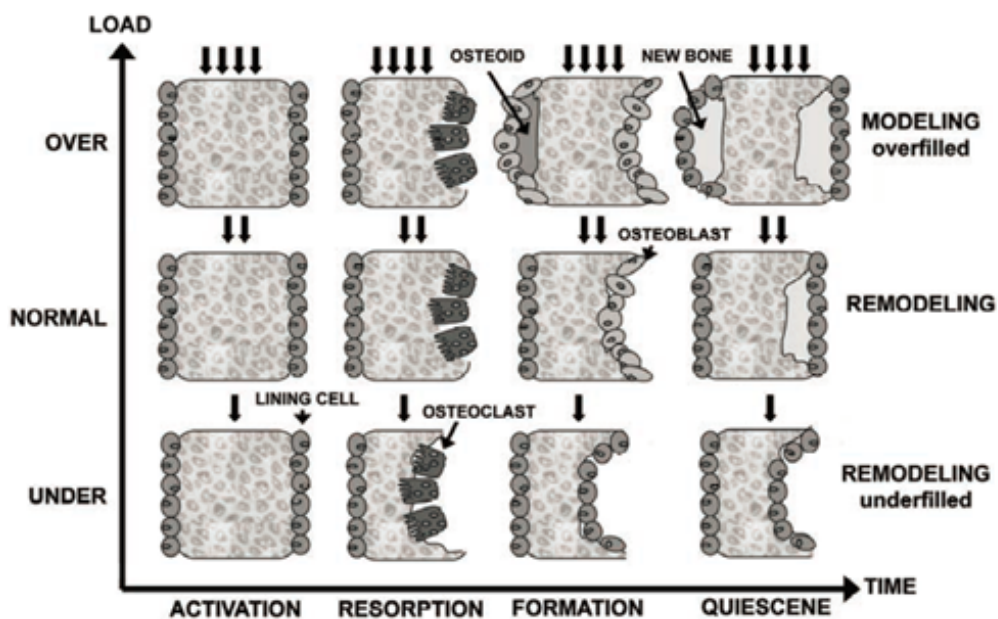
Figure 2.3: Remodeling overview [7]

The typical case for remodeling of the bone is a tooth loss when there is not placed implant right away. Firstly, the loading state of the bone is changed. Secondly, the resorption takes place, and the bone mass decreases. If we want to prevent this scenario and prevent the bone mass decreasing, we need to apply to load (stress) to the bone, which is similar to the state with the original tooth. The most suitable way to do so is placing a dental implant that would have similar mechanical properties as the original tooth. [7]

2.4 Young's modulus of the bone tissue.

The determination of the mechanical properties of trabecular bone is much more complicated than cortical bone. It is mainly because of spongional character. For this reason, it is complicated to determinate Young' modulus of whole trabecular bone.

Therefore, the connection between the architecture of rods and plates and macroscale mechanical properties was studied to analyze the predisposition of fracture. The knowledge of these properties is vital for bone - implant integration. Features of bone tissue are affected by various conditions such as physiological and pathological. Differences in age, species, and diseases, which subject underwent, relate to these characteristics. [8]

As we mentioned earlier, Young's modulus is connected tightly with the density of bone. There have been many studies based on destructive or non destructive tests of bones. Wu and his team reviewed and summarized the trabecular Youngs moduli reported in the literature. The range is quite vast according to bone type, because of that I focused on the trabecular and cortical bone of the mandibular condylar (bone of the lower jaw) [8]. The range of cortical bone was obtained from the Schartz-Dabney study[9] and review by Verplancke and his team. [10]

Trabecular bone of the lower Jaw [8]

- E = 2,71-9,1 GPa

Cortical bone of the lower Jaw

- E = 12,7-22,8 GPa with the mean value of 17,9 GPa according to Schartz-Dabney[9]

- E = 11,3-23,4 according to Verplancke and his team[10]

THIRD

ADDITIVE MANUFACTURING

As we mentioned before, it is a process of joining materials to produce objects from three-dimensional model data. The basic explanation of the method is laying one layer upon another, but there are many various approaches. The most well-known and efficient powder-based high energy additive manufacturing methods are directed energy deposition (DED), selective laser melting (SLM) and electron beam melting (EBM). We use these procedures to obtain stable structures through melting and solidification for load-bearing applications. However, more complex mesh design method are of great interest, especially in the field of tissue engineering.Worth mentioning is that not just powder-based material can be as feedstock materials but also wire-type materials. A typical beginning of all AM techniques is the utilization of geometrical data contained in a 3D model. It is sliced into layers along the z-axis in a virtual environment, and then for each slice, a machine-specific tool path is generated, then an electron beam or high powered laser follows the sliced pattern and melts the powder. Heated pools cool down quickly after melting and solidify in the final form. This process continues with the next layer until the whole structure is completed. [11]

The procedure DED is used usually for the repair of existing 3D models from metal or alloys. The conventional apparatus for DED consists of a head for material powder supply which can position itself by multiple axes and an electron beam projector or high power laser which melts powder through directing the height of power radiation. It is also known by name – Laser engineered net shaping, 3D laser cladding, and directed light fabrication. The main advantage of directed energy deposition is its accuracy and high resolution of the microstructure. The depositing material can be controlled to a great extent, which allows us to produce fine pieces of 3D parts. The problems are great time-consumption and limitation of possible materials. What is more, there is no possible improvement to this method. These disadvantages make it inapplicable for mainstream industrial productions. [11]

As we mentioned earlier, SLM is selective laser melting. The main difference between DED and SLM is the way to feed powder materials. During SLM, the powder is uniformly
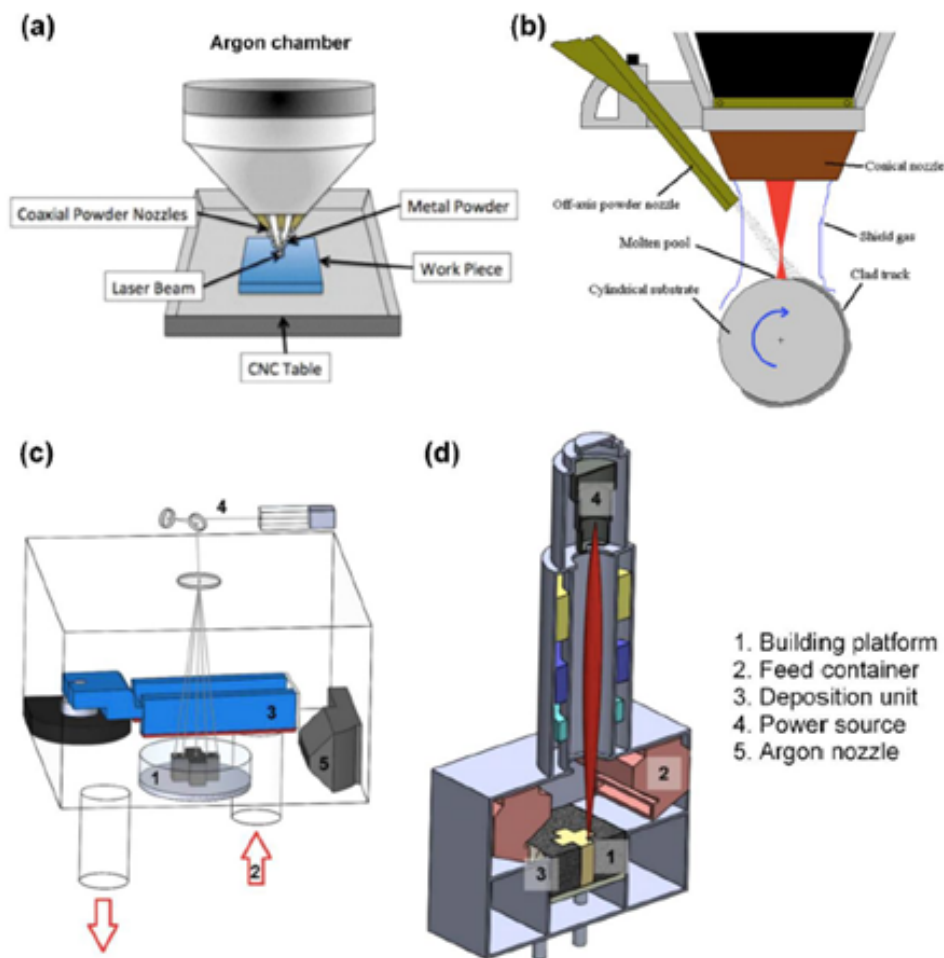
Figure 3.1: (a) Directed energy deposition (b) Directed energy deposition on a tube substrate also known as laser cladding (c) Selective laser melting (d) Electron beam melting [11]

spread in a defined layer on the platform instead of supply from the head. At first, the data from the model are transfer into the platform system and virtually sliced in layers with a defined laser path. The slices are fused layer by layer over several hours to make the final model. This gives us the possibility to design porous and dense metal components. The whole process takes place under inert Argon gas to prevent oxidation and contamination. One significant advantage is the variable surface, which can compromise the aesthetic and technical function. The non-melted powders are left in the powder bed to support the subsequent layers. The other advantages are the elimination of time-consuming and costly furnace post-treatments for debinding, infiltration, or post-sintering. It is also suitable for immediately producing fully dense parts. As a disadvantage, we can count the requirements of high laser power and excellent beam quality. Also smaller scanning velocities (longer build times), melt pool instabilities and high residual stresses are factors which we have to be cautious about when we use this particular method. [12] [13]

At last, EBM is also a powder bed fusion process, but for melting is used electron beam instead of a laser beam. It requires a unique high-vacuum environment due to the special working nature of the electron beam. It provides us an ideal contamination-free environment for manufacturing. What is more, the velocity of the building is faster than DED and SLM due to high energy and fast scan speed. The disadvantage is poor surface quality. [11]

3.1 Porosity

All techniques of additive manufacturing can produce a dense structure with minimal porosity due to production factors. However, sometimes the porosity is requested because, by changing porosity, we can modify the mechanical properties of the structure. For metal alloy Ti6Al4V, which has excellent mechanical properties, we can use pores to prevent "stress shielding effect" in load-bearing implants and to minimalize the impact as much as possible, but we have to mention those non-optimal deposition parameters can cause unwanted porosity which can affect final behavior of implant. [11]

A stress shielding effect occurs in the barrier between bone and implant. For example, let us discuss the loading of the femur. Typically, the femur carries the external load by itself. The load is transferred from the femoral head through the femoral neck to the cortical bone of the proximal femur. Initially, the load is carried by the bone, but when the implant is placed, it participate in the load transmission. The result of participation is that bone stress is reduced and thus stress shielding occurs as shown in the figure 3.5.
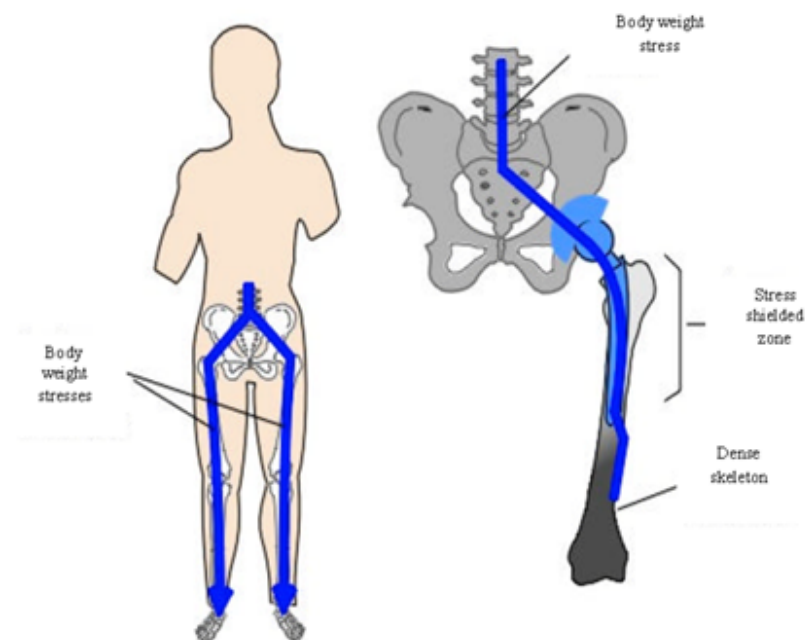

Figure 3.2: the simple scheme of stress shielding [14]

On the contrary, the other end of the femur is overloaded. According to Wolff's law mentioned above, bone transforms in time based on the change of loading state. We can state that the upper part of the femur decreases bone mass after the application of an implant, whereas the lower part of the femur responds by increasing bone mass. Decreasing in bone mass could lead to failure of the implant. [14]

Uncontrolled porosity is very common in addictive manufactured parts. According to a study led by Leuders et al. [15], uncontrolled porosity in specimen could reach 0,23%. Kasperovich and Hausmann reported that the porosity of 0,08% could be achieved by optimization of SMLn [16]. The porosity was scanned by using the X-ray tomography. The porosity of EBM specimens was also measured. The porosity of 0,17% was found in products of the EBM method. The range of pore size was from 50 μm to 300 μm. By using the DEM process, it was found that porosity can be just about 0,01% and the diameter of pores ranges from 1 μm to 3 μm in diameter. If we want to get rid of pores, addictive manufactured objects are submitted to post-processing. The most effective way to reduce the pore volume fraction is hot isostatic pressure. For example, the pore volume fraction was decreased from 0,08% to 0,01% after HIP. [16]

3.2 Effect of pores size on bone ingrowth

Pore size does not only affect the stress shield effect which can lead to bone resorption as we mentioned in the previous chapter, but also the bone ingrowth. This fact is essential for the efficient insertion of the implant. It directly affects mechanical properties, permeability, biological performance and lowers the possibility of implant resection. In recent years, many studies have been focusing on the topic. Bragdon and his team showed that porosities higher than 40% are sufficient for satisfactory vascularization and bone ingrowth [17]. The next study which was led by Murphy stated that the minimum pore size of the implant has to be 300μm for a similar effect [18].

Various other studies are based on pursuing the most effective pore size and pore shape concerning the bone ingrowth. They controlled the porosity and size of pores accurately with the aid of CAD modeling and SLA technology. They observed that the average curvature was reported to induce higher tissue amplification. [19] The other study led by the Taniguchi and his team focused on the effect of the pore size on bone ingrowth in rabbits. They manufactured 3 groups of titanium implants with a pore size of 300, 600 and 900μm. The most effective turn out to be implanted with a pore size of 600μm concerning fixation stability and compressive strength in the early stage of implantation and the highest level of the bone ingrowth in the later stage. [20]
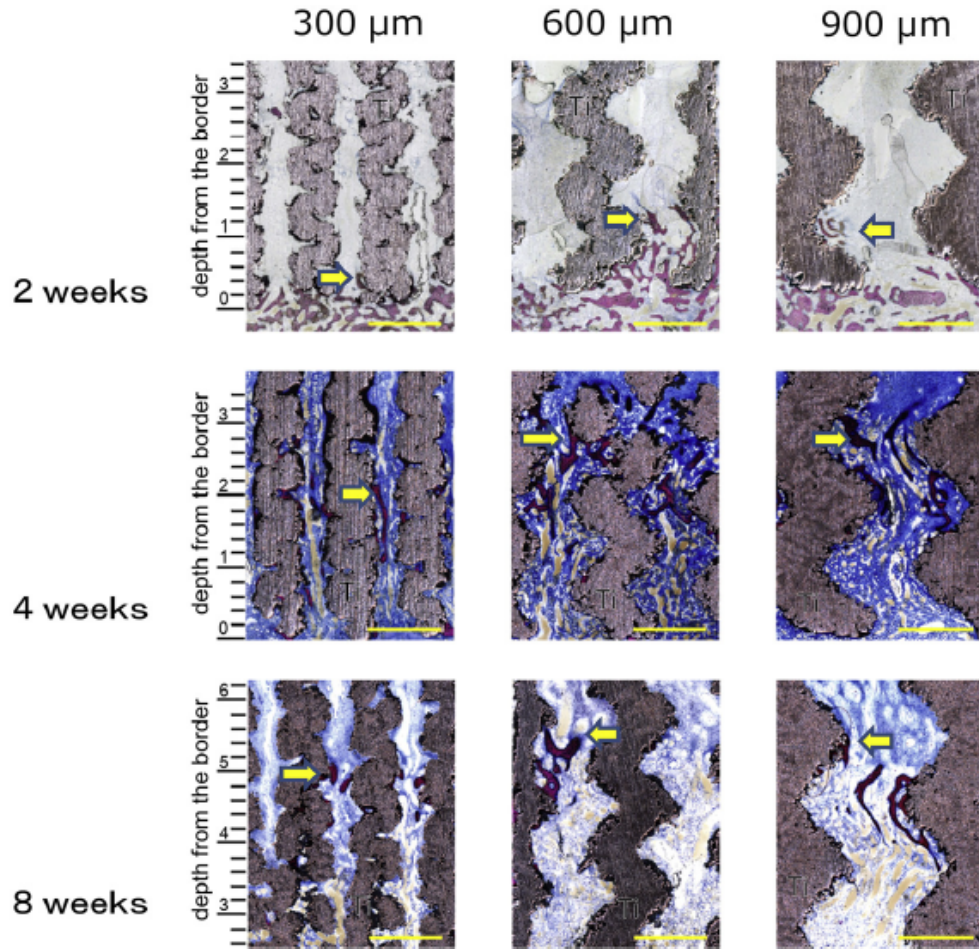
Figure 3.3: In the figure, we can see the section of the titanium implant with different pore size after 2,4 and 8 weeks. We can see the difference in the level of implantation in regards to the pore size. Arrow points the level of bone ingrowth. The purple colours symbolize the presence of the bone and the silver is titanium implant.[20]

3.3 Materials used for 3D printing of the implants

The design and selection of a biomaterial depend on its specific application to be useful and assure its properties as long as required, without rejection. It had ther ato be established properties, which every biomaterial must possess. The material needs to be biocompatible, biofunctional, sterilizable, bioactive or bioinert. Besides, during the process of hygienize and sterilization, it cannot change the fundamental propertiess. If we modify the properties of an implant, we can improve the interaction of the living tissue with its surface. [21]

In the recent few years, the influence of biocompatibility has changed. It was believed that implant should be utterly inert to the human body, without any reaction from the biological medium to its presence. This idea was abandoned when it was observed that any material always provokes a reaction of the living tissue.

Furthermore, the response depends on the age, sex, experienced diseases, etc. of the patient. As a result, there have been studied various types of responses of the living tissue to the implant. [21]
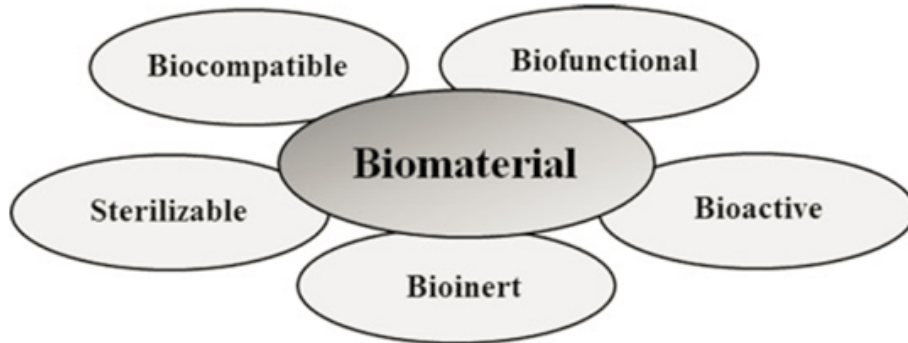

Figure 3.4: Characteristics that material must present to be a biomaterial [21]

The use of medical implants increased in the last decades because of the prolongation of life expectancy, lifestyle, and development of medical technologies. The improvement of biomaterials has been set as one of the majored challenges in the scientific field across medical and engineering areas. All materials which prone to be used as a biomaterial should have specific characteristics in order not to stimulate or cause any level of an allergenic or inflammatory response to the human body. They must be taken into consideration during the developing of a new implant.[21]

Biocompatibility refers to the level of acceptation of the foreign matter in a body and admitting it as part of itself. The immune response is so complex that it is not adequate to describe the biocompatibility of one material to a single cell but as a relation with the whole system. Biocompatibility testing is a compulsory requirement to obtain regulatory approval for the marketing of a medical device. It is essential to follow a strict testing protocol to avoid delay a product launch. [21]

The term biofunctionality describes the essential characteristic of the implant to perform certain functions that need to be fulfilled for the required time. It cannot degrade in contact with tissue. For example, some metal alloys prone to corrode in time, which could cause harmful effects to the body at a certain level. What is more, the material should keep its mechanical and chemical properties during its lifetime. [21]

In summation, we can conclude four different types of materials towards the response of the body. There are bio-tolerable, bioactive, bioinert and bio-degradable. [21]

3.3.1 Bio-tolerable

Human tissue can tolerate these materials. Usually, they are metal alloys. The most known is based on cobalt, chromium, molybdenum, gold or other stainless metals. In general, these materials have excellent material properties. When an implant is placed, we can see

a typical process for bio-tolerable materials, when fibro-osseous integration takes place. The human body develops connective collagen tissue with the variable thickness between the implant and the bone. For implant design is vital to mention that the mobility of the implant is higher than the natural mobility of the tooth. This fact can lead to an early loss of the implant. The medical community took this fact in an account, and these materials are used mainly for short-term implants. The most common problem of bio-tolerable materials is corrosion. Metal ions can penetrate human tissue and could be toxic to the human body. Furthermore, ions pervade further to the body, which could cause metallosis. [22]

3.3.2 Bioinert materials

Bio-inert materials do not cause any organism reaction and it accepts them fully. If they are correctly placed, the surroundings of the implant heal itself by the osseointegration. This process means that the human body produces thin collagen tissue between the bone and surfaces of the implant. We can mention titanium, tantalum and zirconium ceramic. Nowadays, the most common material is titanium and its alloys. This fact has many reasons, and I want to mention several of them [22]:

- High mechanical durability

- High corrosion resistance -After seconds, the passivation of the titanium takes place, which means that a thin layer occurs on the surface of the titanium. What is more, It guarantees the bioinert behavior of the implant.

- The existence of oxygen ensures the high biocompatibility of titanium. We can improve the properties of an implant from titanium by surface treatment, so we achieve optimal osseointegration.

- Titanium is not toxic nor carcinogenic and does not cause any allergic or sensible reactions.

- It has a bacteriostatic effect, which is caused by a thin layer of titanium oxide.

- Various possibilities of forming an additional surface modification are available by modern technologies.

3.3.3 Bioactive materials

Bio-active materials were developed approximately 40 years ago. These materials can make chemical bonds with the bone by releasing ions of calcium and phosphate. This process was named bio-integration. Materials labeled as a bioactive are for example calcium phosphate, hydroxyapatite ceramics, tricalcium phosphate and tetracalcium phosphate ceramic, bioactive ceramic. The effective use of these materials is as an augmented material.
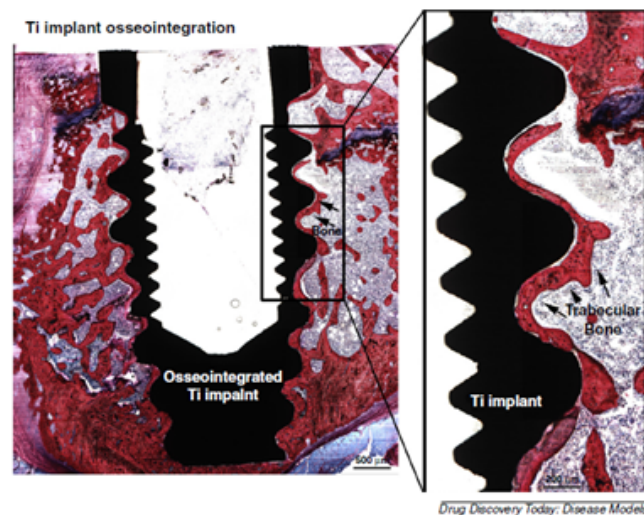
Figure 3.5: Osseointegration of a titanium implant after eight-week implantation [23]

In other words, we apply a thin layer of hydroxyapatite ceramics on the implant to improve osseointegration. On the one hand, we apply a smooth layer in contact with the gingiva. On the other hand, we use a porous layer in contact with the bone. The disadvantage of the method is the instability of the layer and its resorption. Lately, if we want to apply this kind of surface modification, we instead use laser deposition. [22]

3.3.4 Bio-degradable materials

These are materials that degrade or are absorbed within the body in a specific time. Recent studies focus on them, because of the needlessness of further surgery to withdraw the implant [22]. What is more, it allows us to equip the bio-degradable material by the drug. This is a new type of drug delivery to the system. A common approach is typical for surgical insertion of the drug before, and after surgery of the implant, whereas if we place bio-degradable material equipped with the drug, the incorporated drug is released into the system in a controlled manner. Many factors influence the release rate, such as the physicochemical properties of drugs, the degradation rate of polymers, and the morphology. This technology offers us to connect the biocompatibility and biodegradability of the material with the efficient application of the drug. [24]

In conclusion, the most used material for dental implants is pure titanium and its alloys, because of mechanical, chemical and biological properties. The effectiveness of the implant can be improved by surface modification, which can generate the optimal osseointegration and prevents metallosis. When favorable conditions are guaranteed, there can be used zirconium oxide or aluminum oxide ceramics. [22]

3.3.5 Surface modification

The demand for the most efficient implant took us to invent the surface modification. It is considered as a promising alternative to improve the biomaterial-tissue intersection and promote better biocompatibility. Surface modification can be the following kinds: physical-chemical modifications and surface coating. We can see the basic overview in figure 3.6.
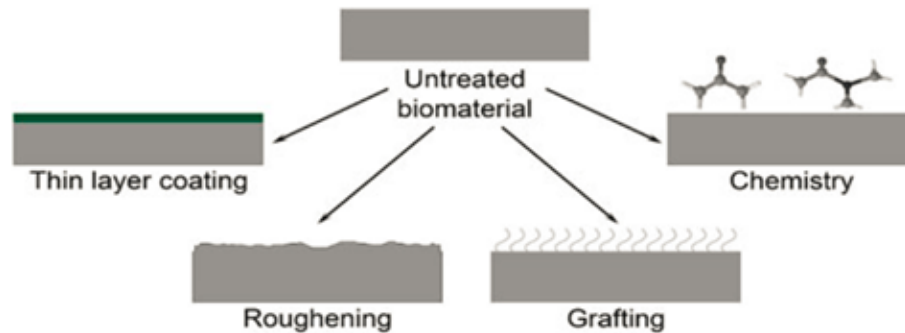

Figure 3.6: Overview of the most common surface modification techniques for biomaterials [21]

Physical-chemical modifications are methods that include the exchange of atoms, constituents, or surface molecules on the surfaces of the implant. Types of physical-chemical reaction could be oxidation (3.7(a)), reduction, acid etching, and acetylation. The physical approach is, for example, grafting (3.7(b)), etching, sandblasting (3.7(c)), mechanical roughening/polishing, and pattering. Under surface coating, we understand the process, where we apply a different material for the layer of the implant. We can mention some of them, for example, grafting, plasma spraying (3.7(d)), non-covalent, and covalent coating, besides thin film deposition. A vast amount of techniques for surface modification can be found in the literature. The problem is that there is not a universal approach to all types of biomaterials. It is based on the desired application and the kind of biomaterial. [21]

3.3.6 Titanium alloy Ti6Al4V

Ti6Al4V alloys are titanium alloys which are typical for excellent corrosion resistance, high fracture toughness, low density, superior biocompatibility, and high strength. It also knows as TC4, and it is one of the most popular titanium alloys used in medical engineering. It makes almost half of the market share of products made from titanium in the world. It was first mentioned in connection with aircraft structural applications because of low weight and high strength. It was used in the construction of jet engines, gas turbines, and other airframe components. Although nowadays the airspace industry is still leading demand for these alloys, other fields of engineering take Ti6Al4V into account.
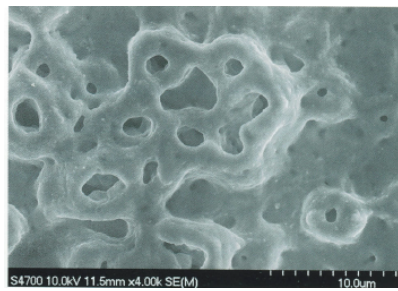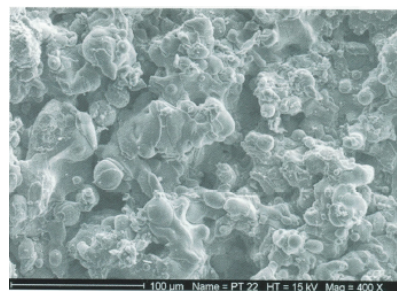
((a)) Anodically oxidized surface [22]
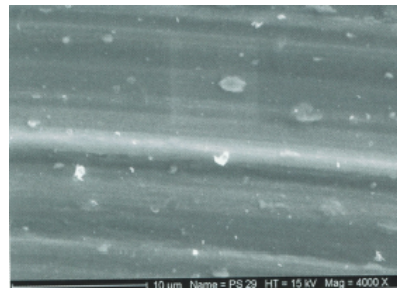
((b)) Titanium surface which underwent grafting modification [22]
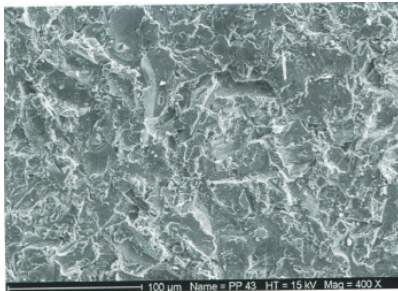
((c)) Sandblasted titanium surface [22]

((d)) Surface modification achieved by the plasma spraying [22]

Figure 3.7: Microscopical overview of the basic surface modification

Automobile, energetic, chemical, and biomedical industries find application for this type of material. Furthermore, the properties mentioned above made it attractive for application as an orthopedic and dental implant mainly due to the excellent biocompatibility. [11] [25]

In spite of high demand, the manufacture is still challenging nowadays because of poor thermal conductivity, the propensity to strain hardening and active chemical reactivity to oxygen. The most used production approaches rely on forging, casting and rolling of bulk feedstock materials. It proceeds to the machining to final shapes and dimensions. The disadvantages of these procedures are a big amount of material waste, high cost, and high time-consumption. These reasons led to advanced manufacturing technology directly from CAD models by adding materials in a layer-by-layer fashion. This technology was named additive manufacturing. It gave is not only a more effective way but also the possibility of fabrication products with geometrical complexities. The figure 3.8 shows us its variability. [11] [25]

3.3.7 Microstructure of additive manufactured Ti6Al4V

Ti6Al4V consists of 6wt% Al and 4 wt% V to pure Ti. Ti is an element which can be found in two different crystal structures: α - Ti and β - Ti. There can be found the structure of α – Ti. It has atoms arranged in a hexagonal close-packed array, and it exists below the β - transus temperature. There is also β - Ti formation, which is a body-centered cubic
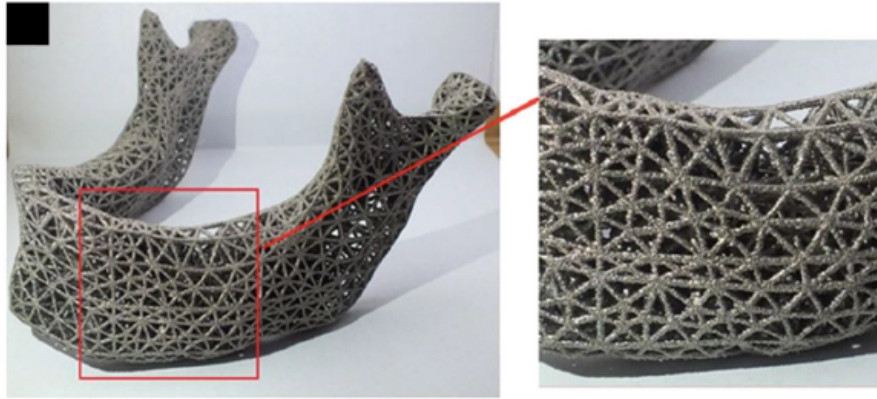
Figure 3.8: 3D mesh Ti6Al4V of lower jaw prosthesis scaffold [11]

(bcc), above β - transus temperature. Aluminium is an α-phase stabilizer while Vanadium stabilizes β-phase. The inner formation of Ti6Al4V alloys is firmly based on temperature history and cooling processes in the fabrication. The $\alpha + \beta$ dual phase exists only under specific circumstances, which includes a slow solidification process. If we have a high cooling rate, β – structure would be decomposed by a non-equilibrium martensite reaction and $\alpha + \beta$ formation won't transform. [11].
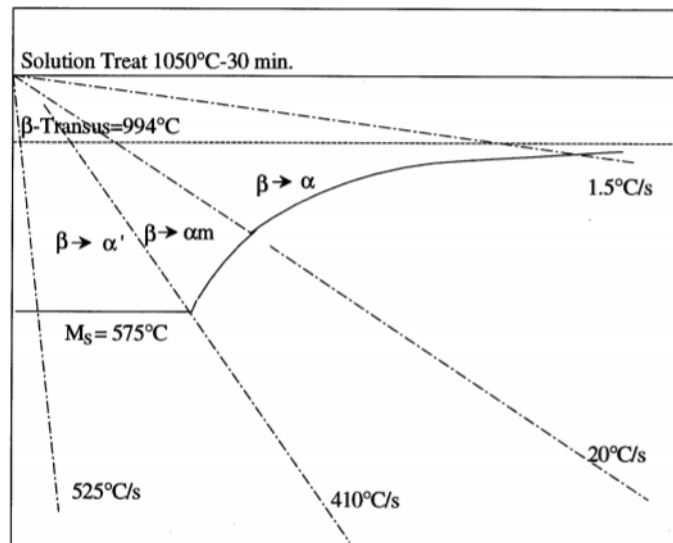

Figure 3.9: Phase transformation as a function of cooling rates [26]

In the figure 3.9, we can see the formation, which we mentioned before. We can find α'-phase named the formation of alpha prime. It is a martensite phase produced by the rapid cooling through diffusionless transformation whereas $\alpha + \beta$ transformation is a diffusional process. There is also a temperature Ms= 575 $^{\circ}$C, which is the martensite start temperature. The martensitic reaction begins during cooling when the austenite reaches the martensite start temperature, and the parent austenite becomes mechanically unstable.

According to the thermal behavior of AM processes discussed above, α' martensite dominates in the production of a microstructure of AM fabricated Ti6Al4V. In the figure 3.10 we can find the optical micrographs of final microstructures in DED, SLM and EBM manufactured Ti6Al4V components. [11]
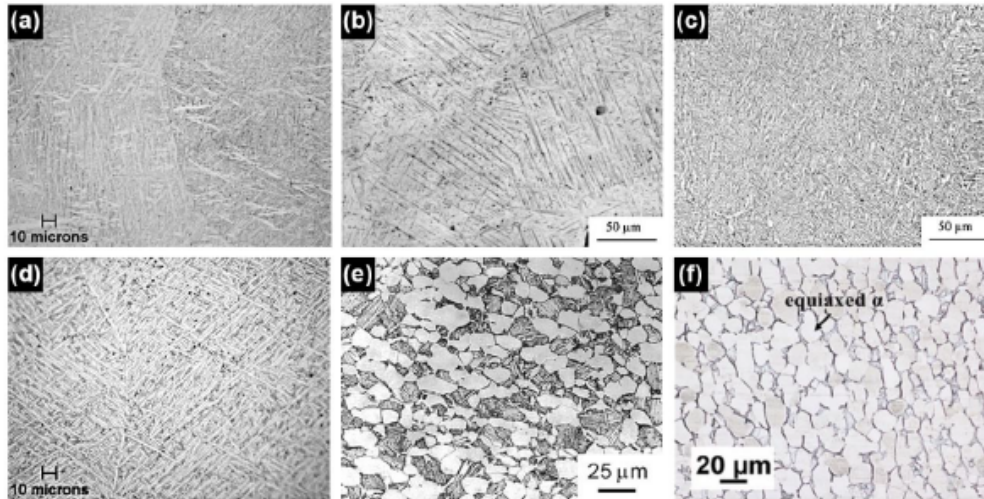

Figure 3.10: Optical microstructures of Ti6Al4V built with different methods (a) Special method of DED with the use of a laser. We can find α' martensite phase (b) SLM method with standard cooling rates produced also α' martensite phase (c) Experimental specimen manufactured by using EBM method has a fine $\alpha + \beta$-phase (d) SLM method with convenient cooling rate gave us $\alpha + \beta$-phase (e) Here we can see microstructure of alloy Ti6Al4V with equiaxial prime α and secondary $\alpha + \beta$ lamellae (f) Equiaxial α colony [11]

FOURTH

TOTAL HIP REPLACEMENT

One of the most significant accomplishments of the modern medical era is total hip replacement, which attaches great importance because it is one of the methods of how to prolong our active lifetime. According to American authors, 306 out of 100 000 men in the age of 65-74 needs a hip replacement. In the case of women, the numbers are 421 out of 100 000 in the age of 75-84. Allegedly, around 10 000 hip replacements are done in the Czech Republic. Under circumstances that the population is getting older, we can expect that this number increases during several years. Nowadays, this procedure is integrated into ordinary orthopedic surgeries. Typically, the cost of implant covers 80% of the final cost of surgery. [27]

4.1 History of knee replacements

In the year 1925, Boston surgeon M.N. Smith – Petersen introduces the new type of hip replacement called "molded arthroplasty." It was a hollow hemisphere made from glass, which was modeled into the shape of a femoral head. It was quite a smooth surface of the implant surface. It is important to point out the fragility of glass. It caused limited durability of the implant. The most significant loading was during walking, which often led to a fracture of the implant. This type of loading was proven to be most crucial for the efficient design of an implant. Mr. M.N. Smith – Petersen continued innovating his type of implant by experimenting with different types of materials such as ordinary steel, polymers, and stainless steel. The next great breakthrough was the invention of cobalt-chromium alloy, which was stainless and quite hard. The procedure, where Co-Cr alloy was used, is called "Smith – Peterson hip cup," which we can see in the figure 4.1. [27] In the end, all methods mentioned above had many disadvantages, for example, low fixing ability to the bone tissue, complicated application for the deformed femoral heads, etc. Nonetheless, these innovative methods opened doors to the new medical areas. What is more, it brought relief to the number of patients. During the 70s, was used "resurfacing of

Figure 4.1: Typical example of the Smith - Peterson hip cup [27]

the hip joint" for the first time. In hip resurfacing, instead of removing the femoral head, It is capped with a smooth metal covering. The damaged bone is removed and replaced with a metal shell. In these days, the most challenge issue was fixing to the bone and the material choice. The ideal material with minimal bone resection, which could preserve the current joint physiology and could be used for non-conventional deformed femurs, was persuaded by producers of resurfacing implant. In the year 1997, the "Birmingham hip resurfacing" was introduced. It was the first replacement, which was authorized by the American nation organization FDA (Food and Drug Administration). For this reason, it was the most successful implant so far. The product spread across the world, but it had one significant disadvantage. The friction between metal articular surfaces of the implant caused complications in the organism, and it was pulled down by several manufacturing companies for this reason. This implant was also available with a newer ceramic head, which guarantees us better surface fixation between implant and bone, but still, the medics and engineers were pursuing a more fitting implant. [27]

The hip replacement was introduced into common medical procedures at the end of the 60s. Since then the procedure innovated rapidly. The basic stayed the same: the joint from a special type of polyethylene (UHMWPE) anchors into the acetabulum and femoral shank from high strength alloy or stainless steel, which is attached into the proximal femur by Polymethyl methacrylate. Parts of femur mentioned earlier can be seen in figure 4.2 . In the year 1958, Mr. Charnley used the current research in the field of new low friction material in the automobile industry, and constructed "low friction arthroplasty." This replacement was typical for an innovative idea to change acetabulum for the artificial socket from modern Teflon. However, Teflon has remarkable friction properties, and the other mechanical properties are not that great. One of them is low resistance against abrasion, and It led to reduced durability. Mr. Charnley decided to change the material of the socket to polyethylene. This was the first efficient total hip replacement.

Mr. Charnley presented the system in 1961 during Sicot congress in Paris, where it was accepted as a general approach for dealing with arthrosis disease for patients over 65 years. Worth mentioning is, the design of Mr. Charnley's implant hasn't experienced dramatic change since then. The original diameter of the metal head was 22 mm, and producers of implants changed it. Nowadays, there are available diameters 22, 26, 28, 32, and 36 mm. During the 80s, there were introduces different materials such as titanium, zirconium, etc., which allowed improving the structure of replacement. Every new improvement prolonged durability and make application easier. These are the milestones of the implant progress. Nowadays, there are various types of hip replacement which I will describe in the next chapter. [27]
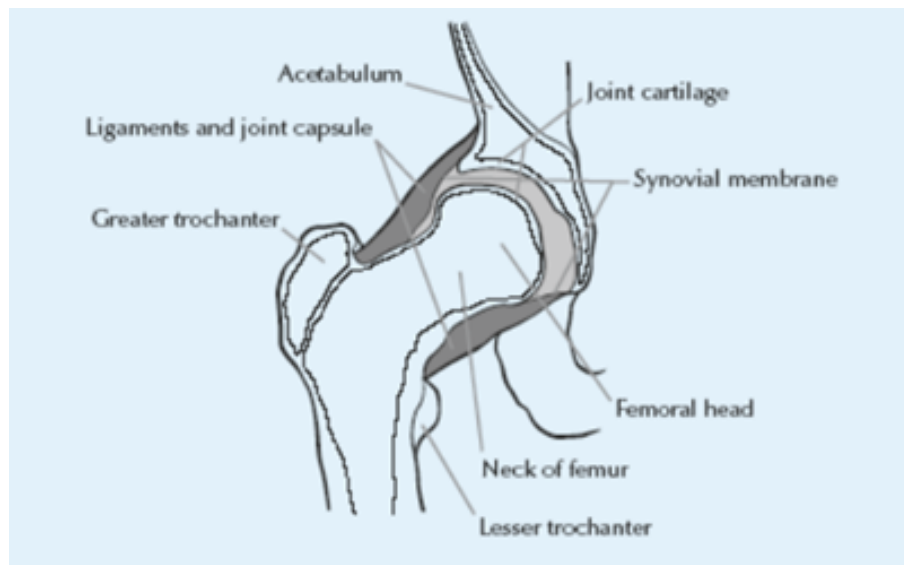
Figure 4.2: Diagram of hip joint structure [28]

4.2 Contemporary types of hip replacements

We can divide hip replacement according to the type of fixation to the bone and size of the implant. If we focus on division according to the size of the implant. We distinguish two main groups: total hip replacement and hip resurfacing. It was mentioned in the previous chapter. If we take into account the type of fixation, we distinguish two big groups, which are cemented implant and uncemented implant. [27]

4.2.1 Hip resurfacing

The main characteristic of hip resurfacing is that the femoral head is not entirely replaced. Instead, the bone is reshaped and covered by the metal prosthesis, and the joint socket is fitted with a metal cup.

As these metal surfaces rub together, there is a threat of release ions. A low level of metal ions does not cause any problem, but the high level could be problematic. This is the reason why many surgeons lost support for these types of implants. The next huge problem is the possibility of fracture below the metal cap on the top of the femoral head. The highest risk is for women with poor bone quality. It is a good possibility for younger people with severe hip problems because it would leave the bone more flexible and available for a postponed hip replacement in the future. Currently, hip resurfacing recommended in instances and for young men with good quality bone. [29]

Figure 4.3: Birmingham hip resurfacing system [30]

4.2.2 Contemporary total hip replacements

The procedure of these implants is characteristic for the replacement of not just the tip of the femur head but the whole part of the upper femur. The first part called "cement total hip replacement" uses cement to fix the implant in the femur canal. The other group uses the mechanical principle of the wedge in the femur canal to place it correctly, then osseointegration takes place to ensure the durability of stability. [27]

Cement total hip replacement

It is a cheaper version of total hip replacement. This method is not recommended to the young people and person with an active lifestyle. Usually, there are made of titan, and there are fixed to the bone by cement, which consists of polymethylmethacrylate. It does not work as a glue but more as a solid interlayer between the inner cortical bone and body of the prosthesis. It is essential for these types of implant that interlayer is stuck to the bone but not implant. The first steps in the research of this procedure tried to have a rigid connection also with the implant, but it led to microfractures, which reduce the durability of the implant. Components of the cement joint prosthesis have circular or oval cross-sections without sharp ends. They have a smooth, sleek or matt surface. [27]
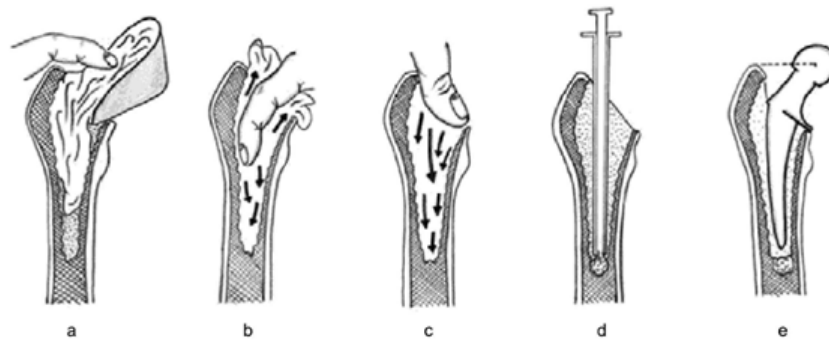
Figure 4.4: Application of cement – a,b,c – 1. Generation of application, d,e- 2. Generation of application structure [27]

Uncemented total hip replacement

During the application of uncemented joint prosthesis, the implant is mechanically placed into the bone without using cement. The period of fixation process to the bone is based more on surface modification rather than the shape of the implant. The process of fixation is called osseointegration, which is described in the 3.3.2 detailly. These types of implants are more common. After an unsuccessful application of uncemented hip replacement, we can use a cemented prosthesis, yet it cannot be applied the opposite way. This makes uncemented total hip replacement a better choice for people with a proactive life because it gives them a chance to achieve full osseointegration around the implant to regain almost full properties of the former state. Whenever the osseointegration does not undergo successfully, we can use a cemented implant to deal with the persisting problem of the hip joint. That is why the uncemented total hip replacement is much more common. [27] We
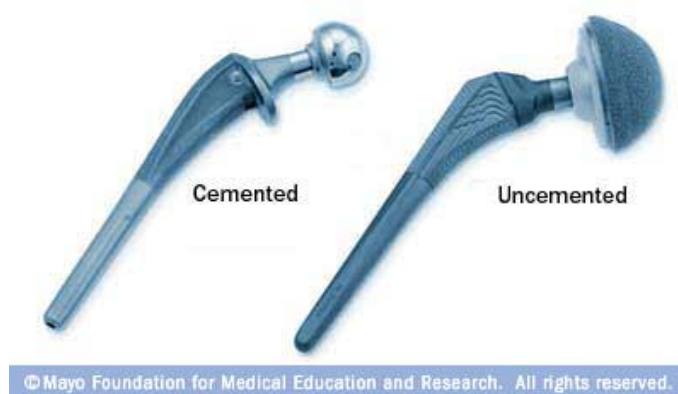
Figure 4.5: Shape difference of total hip replacement [31]

distinguish three different types of stability of implant [27]:

- Primary stability – It is implant stability right after the procedure, and it is affected by the implant shape. This is mechanical fixation and it takes 3-6 months until proceed to the secondary stability. There can also be a case when primary stability is long-term when the osseointegration was not successful.

- Secondary stability – The essential factor for the long-term fixation of the implant is influenced mainly by surface modification. If we choose the type of modification right, the osseointegration is completed, and the connection between implant and bone is fast. The more similar is the surface of the implant to the bone surface the better and more efficient connection is. What is more, if we place a layer of hydroxyapatite on the surface of the implant, we can increase the probability of complete osseointegration.

- Tertiary stability - within several years after the operation, we can see the remodeling of the bone. It is based on the difference between the loading of the bone before and after the operation. On the one hand, the bone gains additional mass in the places with higher stress. On the other hand, the bone reduces mass in the place, where there is lower loading stress after the operation.

As we mentioned earlier, the typical demanded property of an uncemented implant is a surface modification. It can be achieved by techniques, about which I write in the chapter. The shape of uncemented implants can be divided into 3 groups [27]:

- With straight shaft - These implants usually have flat rectangular cross sections with relatively sharp edges or circular cross-sections. These implants fix themselves as a wedge in the bone cavity

- Anatomical shaft – They follow the shape of the femoral canal as much as possible. Thus, it has a circular or oval cross-section in different levels of the length of the implant. Primal stability is achieved by the most accurate filling of the femoral canal, so we distinguish implant for the left and right hip.

- Custom made shaft – We can also make custom made implants according to the RTG model, which encounter technical problems during prefabricating of these implants and cost without any big advantage.
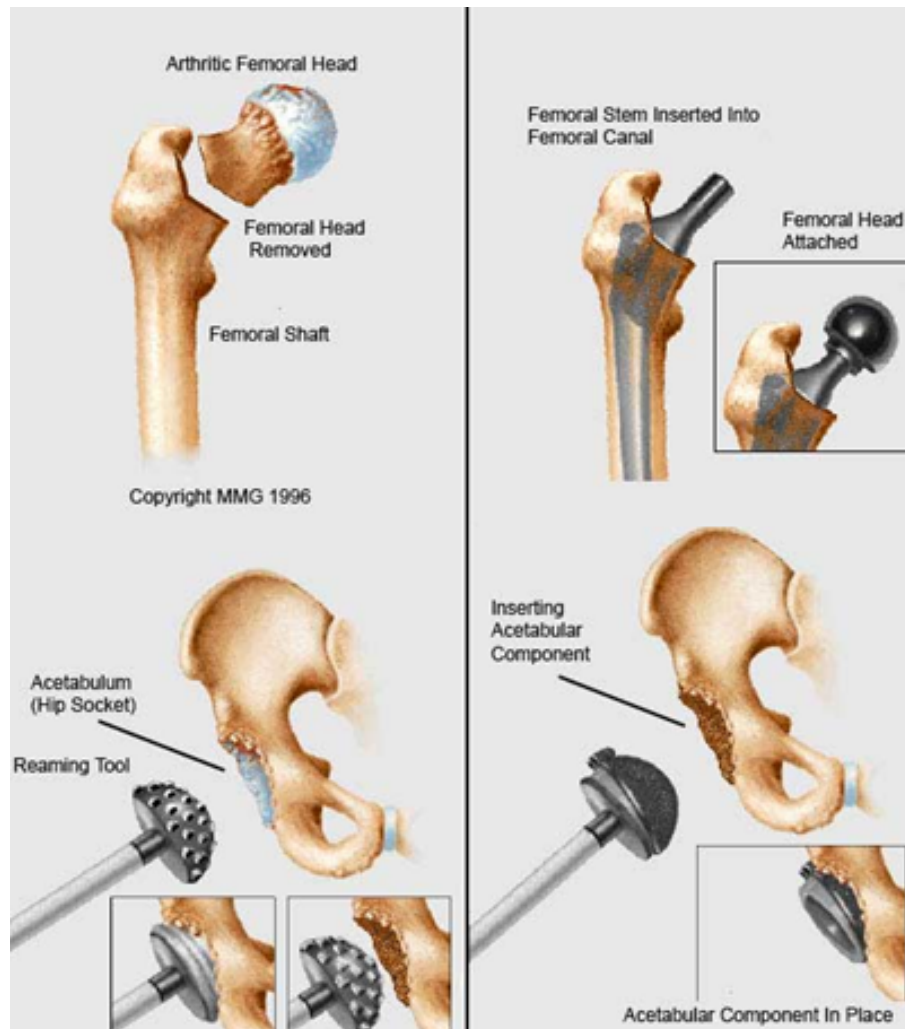
Figure 4.6: Application of the uncemented total hip replacement [29]

KNEE REPLACEMENT

This procedure is often called alloplastic knee replacement. It is the replacement of the knee joint with artificial material. The most common is metal, plastic or ceramic. This procedure is necessary when the knee joint does not have required mobility and cause significant pain to the patient, because of inflammation or injury. In the Czech Republic, the number of operations has reached a few thousand a year. It was surveyed that the success rate is usually about 95% in 5 years after the operation. For an anatomical overview of the knee look at the figure 5.1. [27]
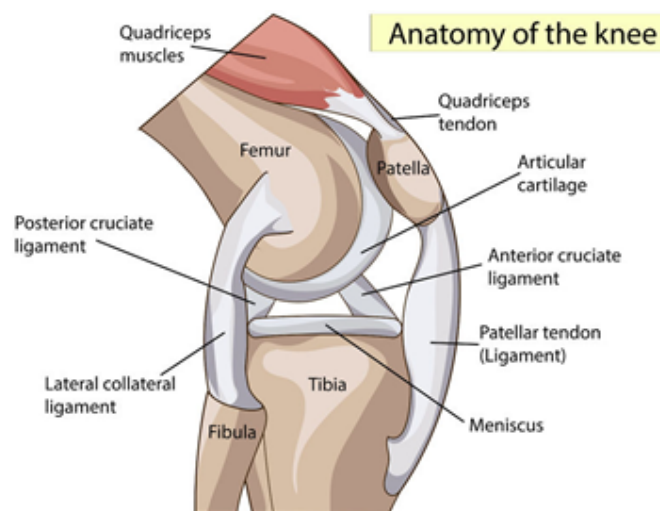
Figure 5.1: Anatomical overview of the knee joint [32]

5.1 History of knee implantology

Searching for the most suitable operation technique to deal with painful knee joint with limited mobility has been pursued since 19. Century. The research of total knee replace-

ment was parallel with the developing of hip replacement. At first, the procedure to regain mobility operated with the tissue of pigs for example muscle tissue, fat or even bladder tissue, which was placed between knee joint surfaces. In the 30s, Fascial graft was used on a similar principle by Campbell. The operation results were not that significant, because of the instability of the knee joint. What is more, the knee regains limited mobility and pain. The first total knee replacement was based on the suspension principle. This implant allowed rotation around one axis, and it was attached to femur and tibia to work as a hinge. The main disadvantage was a high level of bone resorption and durability of the component. Besides, the fixation to the bone was problematic. The prototype was made by Waldius and Shiers. Nowadays, this procedure is used mainly for temporary total knee replacement and also for a patient with deformed bones. A different principle was introduced by McKeever (1957) and MacIntosh (1964) when they used a metal plate between joint surfaces. In 1968, Canadian orthopaedist Frank Gunston used contemporary success in the field of total hip replacement and designed cemented metal joint prosthesis. We can see it in the figure 5.2. This prosthesis consists of two metal hemispheres and two polyethylene tibial components, to respect knee physiology as much as possible. As we said earlier, tibial components were fixed by cement in the bone cavity. Due to the small contact areas, there was highly concentrated stress, which led to short durability. [27] At

Figure 5.2: Gunsten partial knee replacement [33]

the beginning of the 70s, Coventry introduced geometric knee. This type of implant enables to maintain Anterior cruciate ligament (ACL), which led to higher stability because the mutual deformation of opposite surfaces was not enabled. Insall made the next step in 1973. He changed the metal hemisphere with concave shapes and expended contact area between them; then he raised the edges on the sides of the contact surface. The implant also had a small metal plate between condyles which led to the even higher stability of the knee joint. Insall made a femoral component from alloys Chromium-cobalt-molybdenum. Other parts were from polyethylene. This type of implant had the knee rotation capacity between 90 to 100 degrees. The higher rotation was not enabled by the construction of the implant, which was improved in the implant called "Oxford knee." It was made by Good-

fellow and O'Conner. It consists of two polyethylene inserts with a metal tibial plate. The stability of the knee was ensured by lateral and anterior cruciate ligaments, which led even to higher rotation capacity. Worth mentioning is that nowadays most prosthesis application require resection of ACL. [27] Nas Eftekhar made the first total knee replacement in 1970. It consisted of three parts, which were femoral, tibial and patellar replacement with polyethylene articular surface, which was fixed to the bone by cement. However, the cement was not permitted by the FDA by 1971. This prosthesis was a massive contribution with the high success rate. Since then, there have been various designs and material modification of this method. Nowadays, there are more total knee replacements than total hip replacements. [27]

Figure 5.3: Contemporary knee replacement [34]

5.2 Types of knee replacements

Contemporary knee replacements has various shapes, forms and modification. If we want to divide this vast group we need to use specific approaches. We can divide types of knee replacements according to [27]:

- Shape match level of the contact surfaces

- The extent of the implant

- Bone fixation

- Contact surface modification

5.2.1 Shape match level of the contact surfaces

We distinguish [27]:

- Non – constrain – It is typed with minimal inner stability of the knee. Basically, the shape of the tibial component is quite plain and the shape of the femoral component is similar to the distal epiphysis (the bottom part of femur). The advantage of this type of implant is that it respects in a vast amount the biomechanical physiology of the knee, but there is a huge stress in the component.

- Semi – constrain – There is better shape similarity of the ends of tibial and femoral components, so the contact area is greater. For this reason, stress is smaller. The difference with non-constrain can be seen in figure 5.4

- Full – constrain - also called "hinged". Both components are connected by a joint around the horizontal axis. The main characteristic is that lateral cruciate ligaments are not functioning, because whole stability is ensured by the joint. Usually, this type of procedure is recommended for a maximum of 10% of all patients.
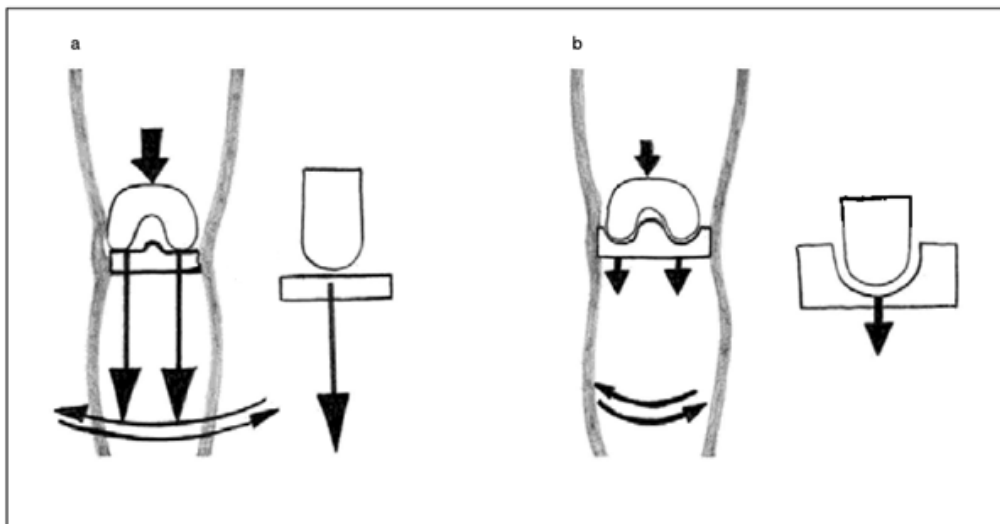
Figure 5.4: The figure of differences between non-constrained and semi-constrained knee replacements a) non-constrained – huge stress on the plate and no inner stability of knee implant, b) semi-constrained – low stress on the plate due to the shapes of components. The is higher inner stability of knee prosthesis. [27]

5.2.2 The extent of the implant

Until recently, there were two groups according to this criterium. They were total replacements and unicompartmental replacements. The unicompartmental group replaced just one half of the knee joint. Usually, it was the medial compartment and condyles of the femur. The main advantage was that the smaller surgical intervention, which led to faster recovery and a smaller impact on the biomechanics of the knee joint. There are quite extensive requirements for this technique for example preservation of ACL and LCL functions, without arthrosis and there cannot be deviation of the knee joint, which quite decreases the number of suitable patients for this type of method. Total knee replacement replaces both halves of a knee joint. [27]

5.2.3 Bone fixation

Unlike total hip replacement, the separation between uncemented and cemented replacement is not relevant, because most of the total knee replacement is fixed by cement. The reason is the success rate and durability of this procedure. However, there is not a high demand for another technique, and we can find few uncemented total knee replacements. The main difference between them is that the surface modification for an uncemented replacement makes the cost of uncemented implant much higher than cemented. [27]

5.2.4 Contact surfaces modification

The pursue more efficient method of the knee replacement pointed out the demand for the most suitable material for contact surfaces. This critical detail requires a material with high rub durability. In the end, this mechanical property could be essential for the durability whole implant, so many producers offer contact surfaces of a femoral component made from Oxinium, Nitride, Titanium or ceramics. Furthermore, they can be necessary for patients with allergic reactions to standard implants. The disadvantage of these knee replacements is the high price, so they are used rarely. [27]

SIXTH

DENTAL IMPLANTS

At first, let us define the field of dental implantology. It is a reconstruction method of the upper or lower jaw by using artificial material, which we insert into the bone or by using unique formed construction which gives us a similar outcome. These methods aim to recover the function of the teeth entirely. The effort of the most suitable reconstruction has been pursuing over a few thousand years, and it encounters a few of the most complicated problems such as the productive reconstruction of the periodontal ligament, adequate replacement of the contact between tooth and gum and the choice of the most suitable material. The most significant step was made in the third problem by using titanium integrated implants with surface modification. [22]

6.1 History of dental implants

The first archaeological discovery of primitive dental implants is from ancient Egypt and before– Christopher Columbus era. We assume that the durability of these implants was quite low. The beginning of the dental implantation is stated between the end of the 19th century and the beginning of the 21st century, and the expansion of science conditioned it. The first pioneer of the field is Magiollo (1809). He installed a small golden tube. There was a tooth initially. Afterward, he used it as a support for an artificial dental crown. In the 19th century, implants were usually made from gold, platinum, silver, iridium, and ivory. Experiments with these materials did not provide satisfying results. Nest step forward was made by Stock (1938). He chose quite a suitable screw-shape which we can see in the figure **??** and it was made from alloy chromium-cobalt- Molybdenum. The problem of this implant is that the alloy is bio-tolerant. [22]

As we mention in the chapter 3.3.1, bio-tolerable materials do not provide the required fixation. Thus the success was not fulfilled. In the year 1947, the Formigini design implant was based on a spiral wire which can be seen in the figure 6.1(b). The revolutionary step was made by using bio-inert material Tantalum. Sweden dentist Gustav Dahl made the

next cornerstone of new dental implants. He was trying to knock down the dental problem by using a new approach. He tried to avoid the complicated foundation of one tooth in the bone. For this reason, he designed complex construction which he placed between the bone and periosteum. A typical example of this dental implant can be found in the figure 6.1(c). Described principle have been not completely forgotten, and it can be found in various cases even nowadays. [22]
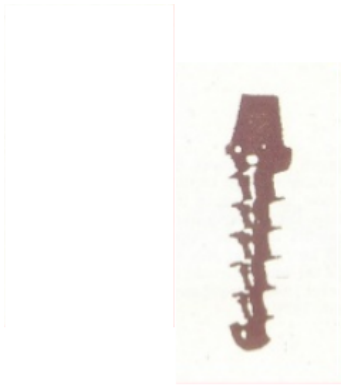
((a)) Stock implant [35]
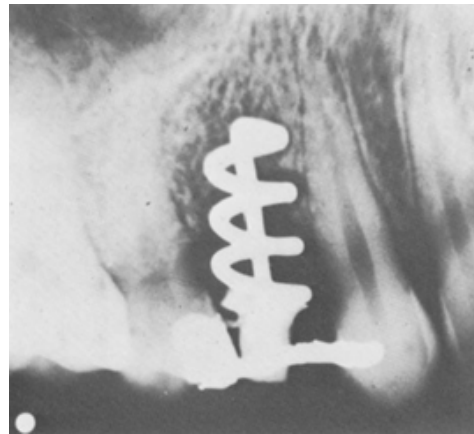
((b)) Formiggini implant [36]
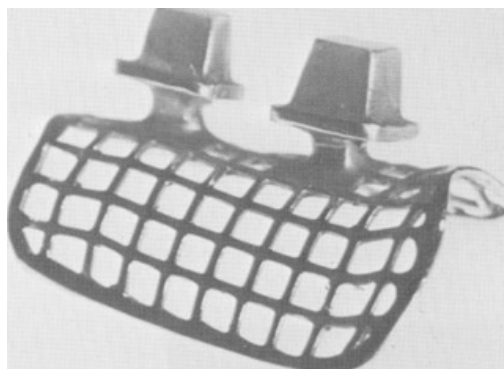
((c)) Gustav Dahl implant [37]

((d)) Brånermark implant [38]

Figure 6.1: Various types of dental implants throughout history

The next achievement in the field of dental implants was made by American dentist Leonard Linkow (1967). He implanted the first titanium blade implant. In the short term, he released a massive campaign for his products. Regardless of the question of durability, the new wave of expansion was launched during the late 60s and beginning of the 70s. In the end, these implants had its significant advantages, but there cannot be sufficiently substituted for original tooth behavior as they were said to be. [22]

Sweden Per-Ingvar-Brånermark made the most significant step so far in dental implantology. The beginning of his work is dated in 1952 when he discovered the osseointegration principle as a young researcher during studies.

It was the basis for modern dental implantology. As we mentioned earlier, the osseointegration principle takes place between the implant surface and the bone. Implant contact to the bone without interlayer of soft tissue. In conclusion, it gives unlimited durability to the implant. Brånermark experimented with screw implants from pure titanium on dogs (1958). Afterward, the first implants from titanium were used as a substitution for the first tooth (1965). In contrast to Leonard Linkow, he did not release the campaign right away and waited 12 years to obtain long-term results of clinical tests with more than 200 test subjects. In the end, he established its exceptional durability and presented results in 1977. His implants took the majority of the market in a few years, and until the turn of the millennium, the osseointegrated implants dominated the market without significant modification. In the figure 6.1(d), we can see typical modern Brånemark root-form implant. Afterward, the dogmatic principle of smooth surfaces as an ideal was questioned, and new surface modification was introduced. The development of rough and porous surfaces gave us a chance to improve the Brånermark method. [22]

6.2 Contemporary types of dental implants

6.2.1 Root form implants

Nowadays, root-form implants dominate dental implantology. Most of them are made from bioactive materials such as pure titanium, titanium alloy or bio-ceramics. It consists of two parts. One of them is a fixture, which is fixed to the bone. The other part includes abutment with an artificial dental crown. Thanks to the bioactive material, the process osseointegration takes place in the surroundings of the screw, which provides high durability to the implant. The fixture could have various shapes, but usually, it is symmetric and cylindrical. According to the shape of the fixture, we distinguish straight-screw and tapered-screw implants, which we can see in the 6.2. If we want to improve its properties, we modify surfaces of implants. Sometimes it is even applied a thin layer of hydroxyapatite to improve osseointegration. Root form implants are the only type, which can be used in every possible indication, but they are quite sensitive to application and oral hygiene. [22]

6.2.2 Blade implants

As we mentioned earlier, this type of implant was developed by Leonard Linkow (1967). Its name is based on the characteristic shape which we can see in figure 6.3. Nowadays, there are made from titanium and companies offer a vast number of various shapes, which provides us the possibility of finding the most suitable implant for the bone of the patient. The blade-shaped body is inserted into the bone. The middle part penetrates the alveolar mucosa, and the upper part of the implant works as a foundation for the artificial dental crown. The first generation of blade implants is placed in one surgery. It includes the blade
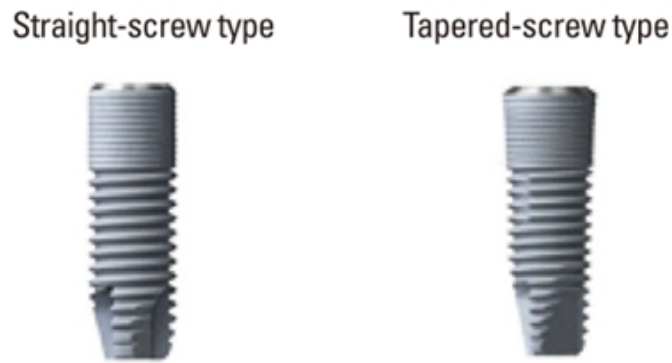
Figure 6.2: Difference between root form implants [39]

part and the artificial tooth so the patient can eat already after the recovery period. The second generation of these implants consisted of two parts, which are placed separately, so it requires additional surgery. [22]
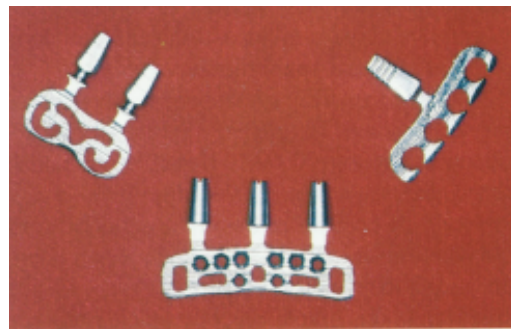

Figure 6.3: Linkow blade implant [22]

At first, the blade part is put in the jaw-bone and let the bone heal itself. The second step is attaching the artificial tooth. The process allows bone surroundings to osseointegrate fully. As we said earlier, blade implants have few significant disadvantages with durability and applicability, yet they have few essential advantages, unlike the root-form dental implants. They are not placed individually but connected with surrounded teeth, and It allows us to operate with teeth damaged by periodontitis. The simple construction of the implant does not prone to technical problems. The application of the blade implant is not as expensive as the root-form implants. It allows us to combinate root-form and blade implants to achieve the most suitable and affordable solution for the patient. We can see the combination in figure 6.4. [22]

6.2.3 Subperiosteal implants

Gustav Dahl firstly constructed the first type of these implants in the year 1940. As we mentioned earlier, he knocks down the problematic of tooth foundation by complex construction which was placed between the bone and periosteum. The artificial crown was
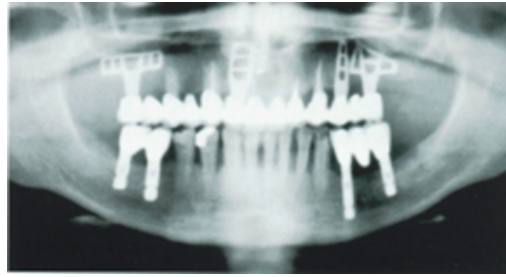
Figure 6.4: Combination of blade-shaped and root form implants [22]

placed on top of this implant. Generally, subperiosteal implants are made from Chromium – cobalt alloys, but nowadays we can make this type of implant from titanium by using the most modern technologies. The typical case for application is toothless jaw or a large gap between teeth. [22]
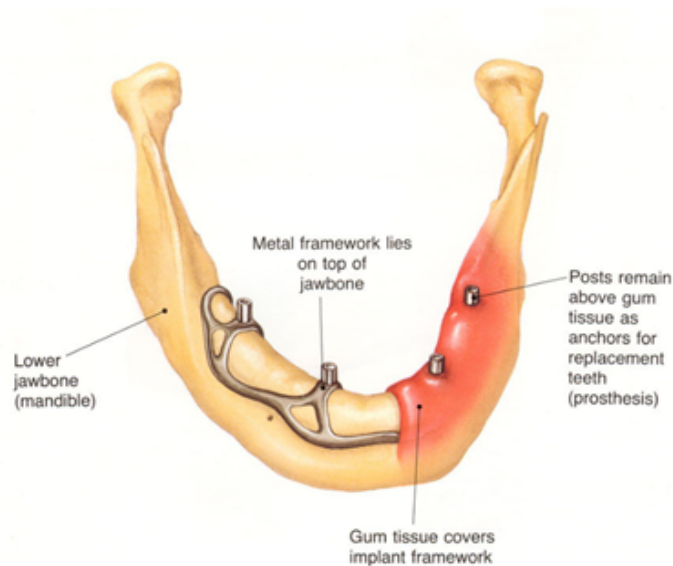
Figure 6.5: Subperopsteal implant [40]

6.2.4 Zygomatic implants

Zygoma implants were first introduced in the late 90s by Dr. Per-Ingvar- Brånermark. The main characteristic of zygomatic implants is the anchoring because it is anchored to the zygomatic bone rather than the upper jaw. Initially, they were developed for a patient without an upper jaw. Nowadays, it is used for dental rehabilitation in patients with insufficient bone in the upper jaw due to, for example, gaining, tumor, toothless jaws or patients with a cleft. They can also be used in the shortened dental arch. The insertion is complicated and quite expensive. [22]
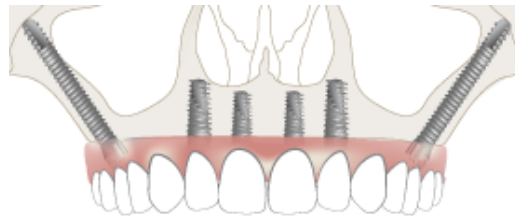
Figure 6.6: Zygomatic implant [41]

6.2.5 Micro implants for orthodontic anchoring

These temporary implants are used for anchoring dental bracelets. They are made from titanium or its alloys. Commonly, the shape reminds us self-tapping screw of 1,3-2,0 mm in diameter. The top of the implant is adjusted to fixing the point of orthodontic wire or spring. When the treatment ends, the implants are removed. [22]

Figure 6.7: Micro implants for orthodontic anchoring [42]

6.2.6 Transdental fixation

Transdental implantation is a procedure of tooth stabilization in the bone of the upper or lower jaw. Indication for use is root fractures, chronical inflammations, and other diseases. They are thin pins from titanium or ceramics. We can also find products that are equipped with a thread at the end of the implant. There are two different approaches to application [22]:

- We insert the implant to the root canal of the tooth which was damaged by periodontitis.

- We insert the implant right through the tooth which was shortened.

The end of the pin is inserted into the bone to a depth of minimal 15 mm. The effectivity of the procedure increases with the depth of the implant in the bone. Anatomical conditions allow us to apply this method for incisors and canine. The success rate is lower than the conventional method, and it is around 80%. [22]

Figure 6.8: Titanium transdental implants [22]

6.2.7 Other types of implants

There are other different implants in use nowadays which we did not mention for example intramuscular implants, which stabilize the total prosthesis. Also, we can find dental implants with the shape of spiral, discs or needle. Contemporary dental implantology is quite conservative, but we can various shapes of implants that can be used if the osseointegration in the surroundings of the implant is successful. [22]

SEVENTH

THE GOAL OF THE THESIS

The aim of the research is the trabecular structure from the point of view of mechanical properties and production difficulties. Although, the trabecular structure can be used for a variety of implants, the thesis focus on dental application. The main goal of the thesis can be described as:

- to design the geometrical model by using plane-based morphology to eliminate the negative consequences of strut-based structures

- to execute mechanical testing of plane-based specimens and compare them with the results of strut-based structure from the previous study

- to develop the numerical model which can correspond with the results of mechanical testing

GEOMETRICAL MODEL

Based on the knowledge in previous chapters, the paper has an objective to design an artificial model 3D- printed microstructure with similar properties as trabecular bone. It could allow us to design an implant that does not need a surface modification which we mentioned in the chapter 3.3.5. We substitute the surface modification by the porous microstructure. This method has a variety of reasons. First of all, there is no universal approach of surface modification to all biomaterial, but the porous structure can be used in all cases of additive manufactured products. The second huge advantage is the control of the pore size. This gives us a chance to optimize the pore size to maximalize the bone ingrowth. In the end, if we change the porosity of the microstructure, we can modify Young's modulus to minimalize the stress shield effect which can lead to resorption of the human bone. This problem is described in the chapter 3.1.

8.1 Contemporary structures

The main goal of the thesis was to design an optimal structure that can withstand maximal loading and also provide sufficient environment to bone ingrowth. In the beginning, there were selected 3 types of strut-type structures that can be generated in software Magics (Materialize NV, Leuven, Belgium). We can see the selected structures in the figure 8.1. Furthermore, the platforms were placed on opposite sides of the gyroid structure for easier mechanical testing. We can see the whole process in the figure 8.2.

The next step was the fabrication of structures. As a material, the titanium alloy Rematitan CL was chosen which was provided by the "Concept Laser" company and the production of samples was done in collaboration with the company "ProSpon spol. s r.o." The process of production took around 2 months. The chemical composition of the material can be found in table 8.1. This type of titanium alloy has a rich history of application as a biomaterial, and it has proven to be efficient biomaterial for variety of application. The material properties of Rematitan are shown in table 8.2. The additive manufacturing

was done by the Selective laser method in the machine M2 Cushing Laser in the protective Argon atmosphere. After printing the structures had to undergo thermal treatment to eliminate the residual stress. It was done in a vacuum furnace where the temperature reached 840°C in 4 hours. Afterward, the temperature stopped for 2 hours and then cooled down to 500°C.

| ((a)) Dode Thick | ((b)) Diamond | ((c)) Rhombic dodecahedron |
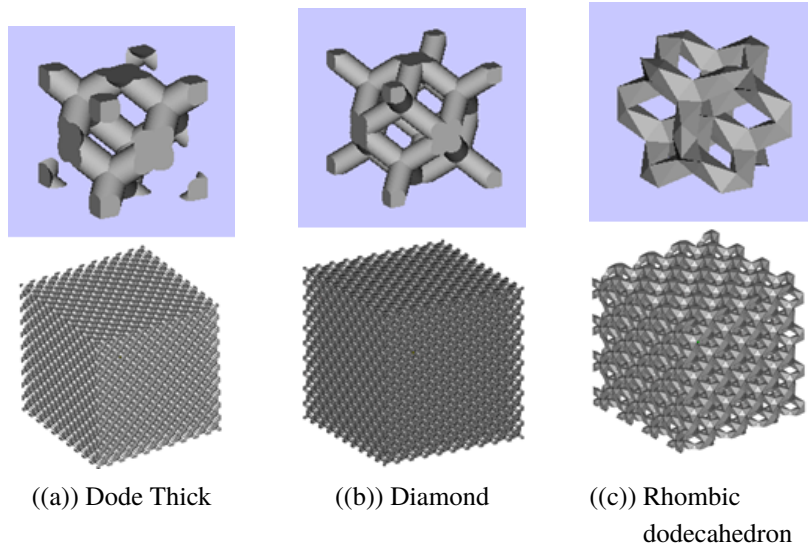
Figure 8.1: Three types of structure were generated in software Magics. In the upper row, we can find basic cells of the structure while in the lower row we can see figures of the multicell matrix of the structure
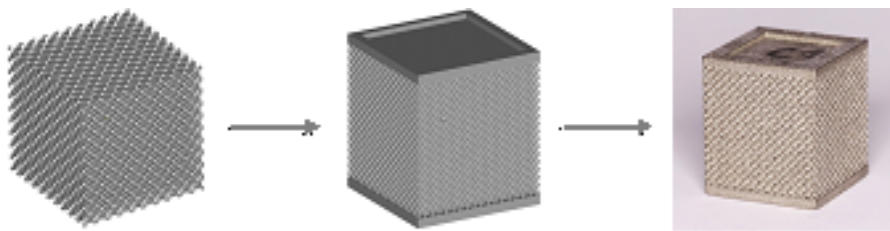
Figure 8.2: The production process

Afterward, the structures underwent visual examination which revealed few defects. The significant defects were in the border area between the trabecular structure and the homogenous part. It is assumed that fractures were made due to thermal expansion. Although the specimen has 2 border areas, the fractures were found just in one. It is assumed when the trabecular part is printed before the homogeneous part, the cooling velocity of the trabecular part is higher than the cooling velocity of the homogenous part. The struts of the trabecular part were shorted in a short time which led to fractures. We can see the fractures in the figure 8.3.

Table 8.1: The chemical composition of the Rematitan metal powder provided by the "Concept Laser" company [43]

Component	Mass(%)
Ti	90
Al	6
V	4
Other elements: N ,C ,H ,Fe ,O	<1%

Table 8.2: Material list of the material used for gyroid manufacturing provided by the "Concept Laser" company [43]

Yield Strength $R_{p0,2}$	900 MPa
Tensile Strenght R_m	1005 MPa
Elastic Modulus E	115 GPa
Melting range Δ	4,5 g/cm3
Density ρ	1604-1655°C
Coefficient of thermal expansion TEC (25-500°C)	$10,16 \times 10^{-6} K^{-1}$
Colour	white
Metal-ceramic bond strength acc. to EN ISO 9693, 3-Pt.- bending test (min. 25 MPa according to EN ISO 9693	37 MPa (Triceram, Dentaurum)
Type	4
Biocompatibility, L 929-Proliferation according to EN ISO 10993-5, -12 toxic active substances	No deliberation of cell toxic active substances
Corrosion resistance, static immersion test according to EN ISO 10271 (max. $200\mu g/cm^2$ x7d according to EN ISO 22674)	Ion release $1,41\mu g/cm^2$x7d

This led to the modification of the loading platforms. The goal of the modification was to reduce homogenous mass as much as possible by cavitis to maximalize cooling velocity. The process of modification can be seen in the figure 8.4. This problem is mainly for specimens which undergo tensile tests. The presented paper deals only with compressive tests. The platforms of our specimens were thin enough to not be influence by this problem.

The next problem was microfractures inside the strut-based structure which were observed. This fracture can split in time and lead to necrosis or aseptic loosing of the implant. We can see the microscopic detail of defects in the figure 9.8(a). It is assumed that
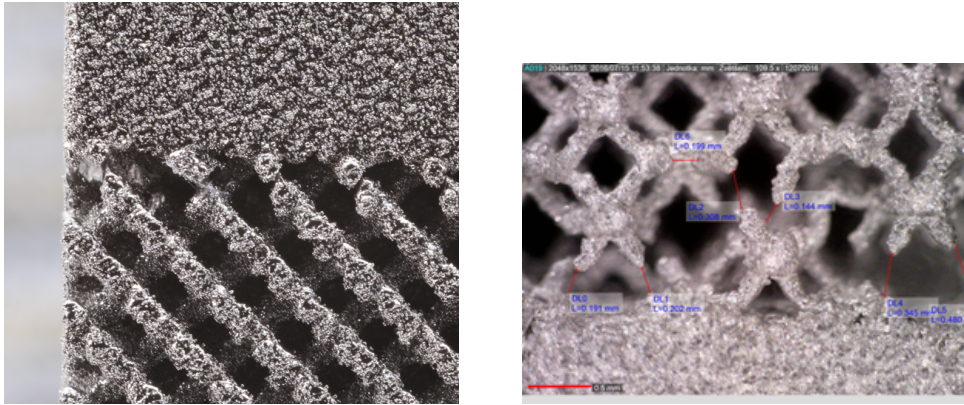
((a)) The detail of the structure border area   ((b)) Microscopical detail of border area

Figure 8.3: In the figures above we can see the fractures due to different velocity of thermal cooling
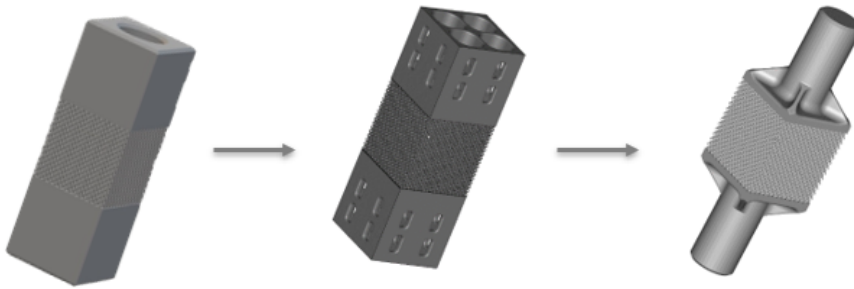
Figure 8.4: The process of platform mass reduction for tensile tests

the problem is due to the strut-based type of structure.

This was the main reason why the plane model was chosen. The gyroid structure was selected for its constant pore size throughout the model. The goal of this thesis was to made 5 gyroid structures of different thicknesses and underwent the experimental tests of all models to verificate the models.

8.2 Geometrical model of gyroid structure

As we mentioned earlier, the gyroid structure was chosen. It is a continuous and triply periodic cubic morphology with a constant curvature surface across a range of volumetric fill fractions. It can be found in a variety of natural and synthetic systems. [44]

The most convenient approximation of the gyroid structure for our purpose is through a level surface. It is defined by the function:

$$F(x, y, z) = t \tag{8.1}$$

, where F determines the form of the surface via space-dividing function and t is a con-

stant which determines the volume fractions of the divided space. If we set the parameter t to zero and substitute the F with an appropriate function, we receive the equation:

$$\sin(\tilde{x}) * \cos(\tilde{y}) + \sin(\tilde{y}) * \cos(\tilde{z}) + \sin(\tilde{z}) * \cos(\tilde{x}) = 0 \qquad (8.2)$$

, where x̃,ỹ and z̃ are scaled spatial ordinates such that x̃ = 2π*x/a, ỹ=2π*y/a, z=2π*z/a. The variable a is the cubic unit cell edge length[45]. There were made 4 types of gyroid structures. All gyroid structures have dimensions 16x16x16 mm. The parameters of specimens can be found in the table 8.3. The last column refers to the criterium of optimial pore size for bone ingrowth. The optimal pore size according to the Taniguchi and his team is 600 μm, which is detailly described in the chapter 3.1. On the basis of previous, It is assumed the range is 450-750 μm. If the pore size of structure is in this range, we state that it is efficient for bone ingrowth.[20]

Table 8.3: The parameters of gyroid structures [20]

Name	Unit cell	Pore size	Bone ingrowth
-	[μm]	[μm]	-
Gyroid structure nb 1	1400	400	out of range according to literature
Gyroid structure nb 2	1800	450	✓
Gyroid structure nb 3	2400	700	✓
Gyroid structure nb 4	3000	850	out of range according to literature

We can see the overview of gyroid structure in the figure 8.5.
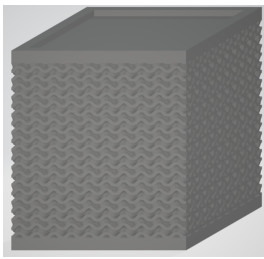
((a)) The model of gyroid number 1
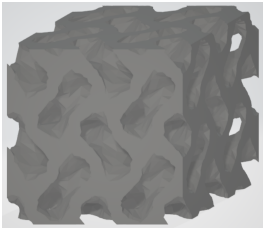
((b)) Unit cell of gyroid number 1
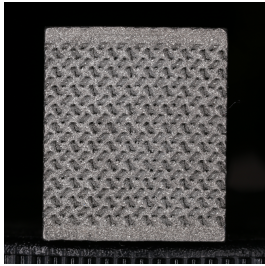
((c)) 3D printed gyroid number 1
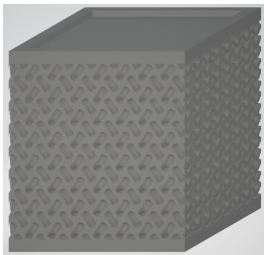
((d)) The model of gyroid number 2
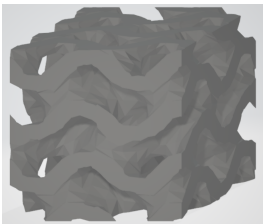
((e)) Unit cell of gyroid number 2
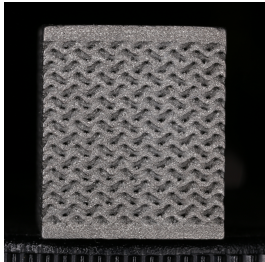
((f)) 3D printed gyroid number 2
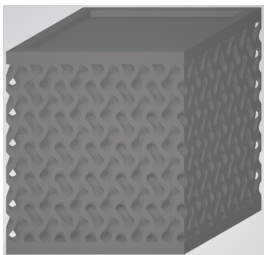
((g)) The model of gyroid number 3

((h)) Unit cell of gyroid number 3
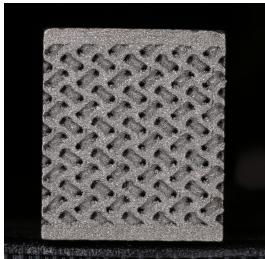
((i)) 3D printed gyroid number 3
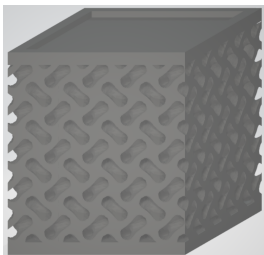
((j)) The model of gyroid number 4
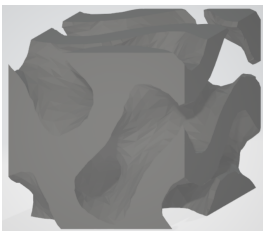
((k)) Unit cell of gyroid number 4
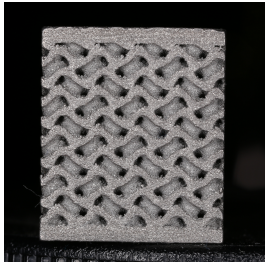
((l)) 3D printed gyroid number 4

Figure 8.5: Overview of gyroid structures - each row displays one type of gyroid. There is photo of 3D printed strucuture, the model of gyroid structure and unit cell of gyroid structure

MECHANICAL TESTING

The gyroid structure underwent which were produced by additive manufacturing underwent compressive mechanical testing. The process of manufacturing was the same as the previous samples. The description can be found in the chapter 8.1. The goal was to obtain material characteristics of trabecular structures and compare them with the results of the numerical simulation, following model verification. The essential material characteristic for our purpose is the **global modulus of elasticity** of each structure.

Mechanical testing was done in the form of pressure tests. There were produced three specimens for each gyroid structure in total 12 tests subjects. Tests were executed according to international standard ISO 13314:2011 *Mechanical testing of metals — Ductility testing — Compression test for porous and cellular metals*. The standard is intended for porous and foam metals with porosity higher than 50%.

9.1 The process of mechanical testing

The faculty of civil engineering CTU Prague posses the machine MTS Alliance RT-30 (MTS, USA), which was used for compressive strength of gyroid structures with the maximal load of 50 kN. The tests were executed in the laboratory at room temperature. The load direction was the same as the direction of additive manufacturing and thus perpendicular to the printed layers. This was important because of orthotropic behavior caused by the technological procedure when the layer is placed upon the other. The specimens were loaded by remote displacement and the velocity of deformation was set to 1×10^{-3}mm per minute which correspond to the standard.

Material characteristics of the trabecular structure were based on stress-strain curves which were obtained by compressive tests. The stress was calculated from the following equation 9.3:

$$\sigma = \frac{F}{A} \tag{9.1}$$

, where σ stands for stress, the *A* stands for the area of gyroid cross-section and *F* stands for the force which is applied perpendicularly to the area of gyroid cross-section where the stress is calculated.

The relative deformation of the specimen was calculated according to the equation 9.4

$$\epsilon = \frac{\Delta h}{h} \tag{9.2}$$

, where ϵ stands for relative deformation, the Δh stands for measured deformation and h is the original height of the gyroid structure.

As we said earlier, the main mechanical characteristic were the global modulus of elasticity (E) for our purposes, then the first maximum compressive strength - $\sigma_{first,max}$ and contractual compressive strength - $\sigma_{0,2}$. The first maximum compressive strength was set as the first local maximum of the stress-strain curve in figure 9.1. The contractual compressive strength - $\sigma_{0,2}$ is defined as the stress in the material when the material reaches the plastical deformation equal to 0,2%. The quasi-statical gradient specified this moment. Furthermore, it was used to determinate the global elastic modulus.
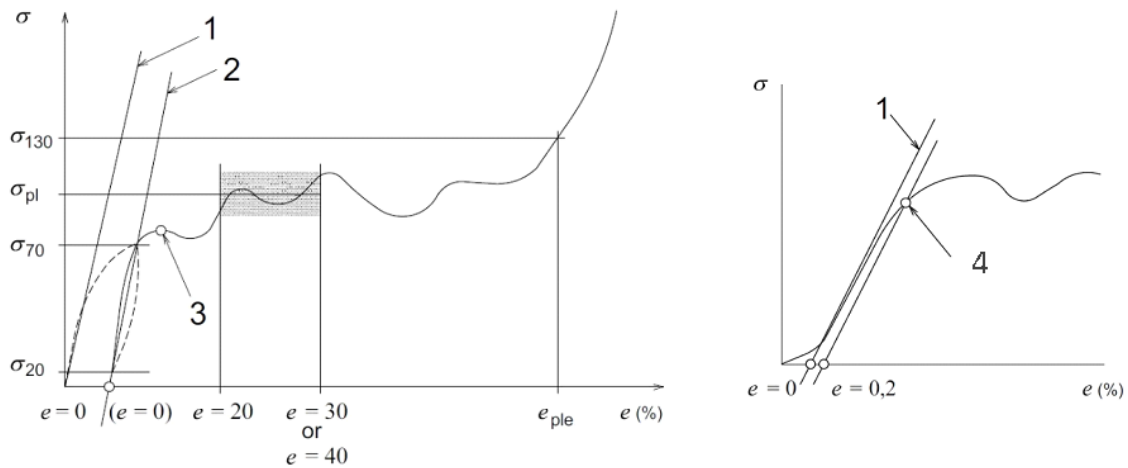
Figure 9.1: The stress-strain curve obtained from standard of compressive testing of porous and foam metals (ISO 13314:2011) with specific characteristics such as 1-quasi-statical gradient, 2- elastic gradient, 3- the first maximum compressive strength- $\sigma_{first,max}$, 4- the contractual compressive strength - $\sigma_{0,2}$

The determination of the quasi-statical gradient can be done as we can see in figure 9.1. According to the figure in the standard ISO 13314:2011, It can be stated that the quasi-statical gradient is defined as the tangent line inclination of the stress-strain curve in the point of inflextion. This point divides the curve into the convex and concave parts. The curve concavity is due to plastical deformation. Numerically, the point of inflexion is specified as the point when the curve inclination starts lowering. It can be calculated from the equation:

$$\Delta E = \frac{\sigma_i}{\epsilon_i} - \frac{\sigma_{i-5}}{\epsilon_{i-5}} \tag{9.3}$$

, where σ_i stands for the stress in the i-step of measurement, ϵ_i is the deformation in the i-step of measurement, σ_{i-5} stands for the i-5-step of measurement and finally, the ϵ_{i-5} is the deformation in the i-5-step of measurement. The inclination change was set after 5 steps to eliminating the error possibility caused by the measurement deviation of the applied force (F) and deformation (Δh),

Although according to the standard, the quasi-statical gradient is not equal to the global elastic modulus, the curve inclination in this point is the most suitable for the global elastic modulus. In the beginning, the stress-strain curve does not correspond with the real loading progress. Behind the point of inflextion, the inclination is significantly influenced by the plastic deformation.

The next step was the determination of the point, which is the intersection of the quasi-statical gradient and the x-axis(e=0). Numerically, the point can be computed:

$$x_0 = -\frac{b}{a} \tag{9.4}$$

, where *a,b* stands for constants of quasi-statical gradient linear equation in the slope-intercept form. When the plastical deformation equals to 0,2% was added(e=0,2), the intersection of the line with the stress-strain curve gives us a contractual compressive strength. The process can be seen in the left graph in figure 9.1. The slope-intercept equation of the new line is define

$$y = a * x + c$$
$$c = (x_0 + 0,2) * a \tag{9.5}$$

where *a* still stands for constant of quasi-statical gradient and also for the global elastic modulus of gyroid structure.

Numerically, the intersection of the mentioned line with the stress-strain curve is the point where the condition is fulfilled:

$$|a * \epsilon_i + c| = |\sigma_i| \tag{9.6}$$

, where σ_i and ϵ_i stands for stress and deformation in the i-step of measurement.
In addition, the last important material characteristic is the porosity of the gyroid structures. Porosity was determined as:

$$n = 1 - \frac{m - (V_{hom} * \rho_{Ti6Al4V})}{A * h * \rho_{Ti6Al4V}} \tag{9.7}$$

, where m is the mass of the specimen, V_{hom} stands for volume of the homogenous part of the gyroid specimen, *A*, and *H* are the dimension of the trabecular structure and $\rho_{Ti6Al4V}$ stands for a density of titanium powder which was used to manufacture the specimen. The porosity was used for comparison between the trabecular structures. It is assumed that the higher porosity the lower other mechanical properties

9.2 The evaluation of mechanical testing

The results of mechanical testing in compression for each specimen are listed in the table 9.1. In the table 9.2 we can find the mean values for all gyroid structures. We can conclude based on experiments that the global elastic moduli of gyroid structures are significantly lower than the elastic modulus of the material Ti6Al4V, which is equal to 110 GPa according to the catalog list. It referred to the state after printing and recommended thermal treatment. Furthermore, the elastic moduli of all structures are close to the elastic modulus of trabecular human bone 2,71-9,1 GPa, which was detailly described in section 2.4. The essential part of the design was to adapt the elastic modulus of the structure to the bone as much as possible to avoid negative consequences which are called stress shield effect. This phenom was described in section 3.1. In the following part, we can see the stress-strain curves for all sets of gyroid structures.

Table 9.1: The results of mechanical testing for each individual gyroid structure

Type of gyroid structure	E	$\sigma_{first,max}$	$\sigma_{0,2}$	n
-	[GPa]	[MPa]	[MPa]	-
Specimen G1-1	3,109	230,343	142,833	0,516
Specimen G1-2	3,136	229,203	190,257	0,521
Specimen G1-3	2,898	225,957	167,878	0,518
Specimen G2-1	2,848	214,831	165,747	0,567
Specimen G2-2	2,897	223,780	156,842	0,574
Specimen G2-3	2,860	205,803	162,074	0,571
Specimen G3-1	2,832	190,789	159,437	0,588
Specimen G3-2	2,841	190,394	156,308	0,594
Specimen G3-3	2,839	190,825	157,546	0,591
Specimen G4-1	2,795	189,748	152,395	0,608
Specimen G4-2	2,763	190,017	127,014	0,611
Specimen G4-3	2,759	194,537	155,592	0,604

Table 9.2: Mean values of mechanical properties for each individual gyroid structure

Type of gyroid structure	E	$\sigma_{first,max}$	$\sigma_{0,2}$	n
-	GPa	MPa	MPa	-
Gyroid structure nb 1	3,048	228,501	166,990	0,518
Gyroid structure nb 2	2,868	214,805	161,554	0,571
Gyroid structure nb 3	2,837	190,670	157,764	0,591
Gyroid structure nb 4	2,772	191,434	154,119	0,608
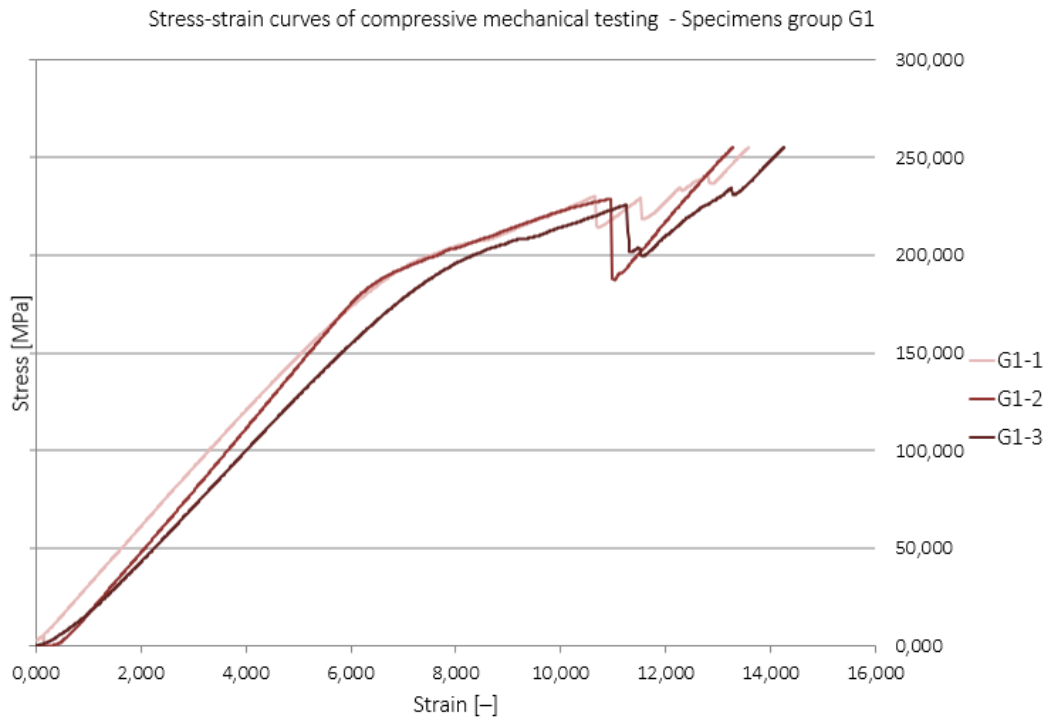
Figure 9.2: Stress-strain curve obtained from compressive testing of gyroids number 1
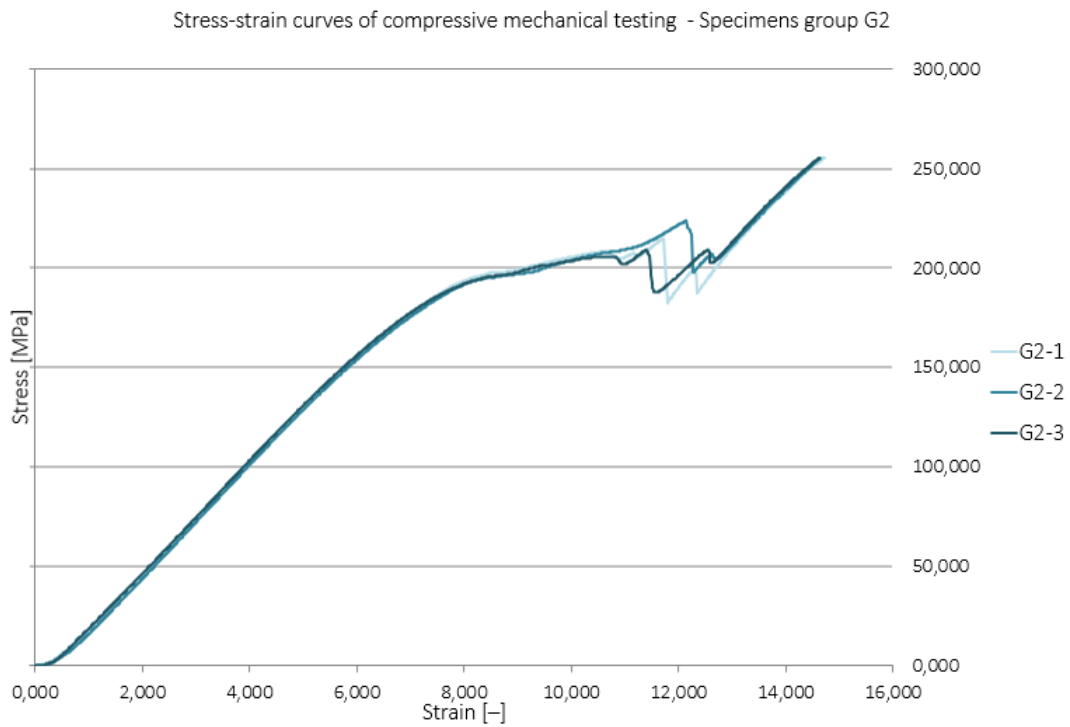
Figure 9.3: Stress-strain curve obtained from compressive testing of gyroids number 2
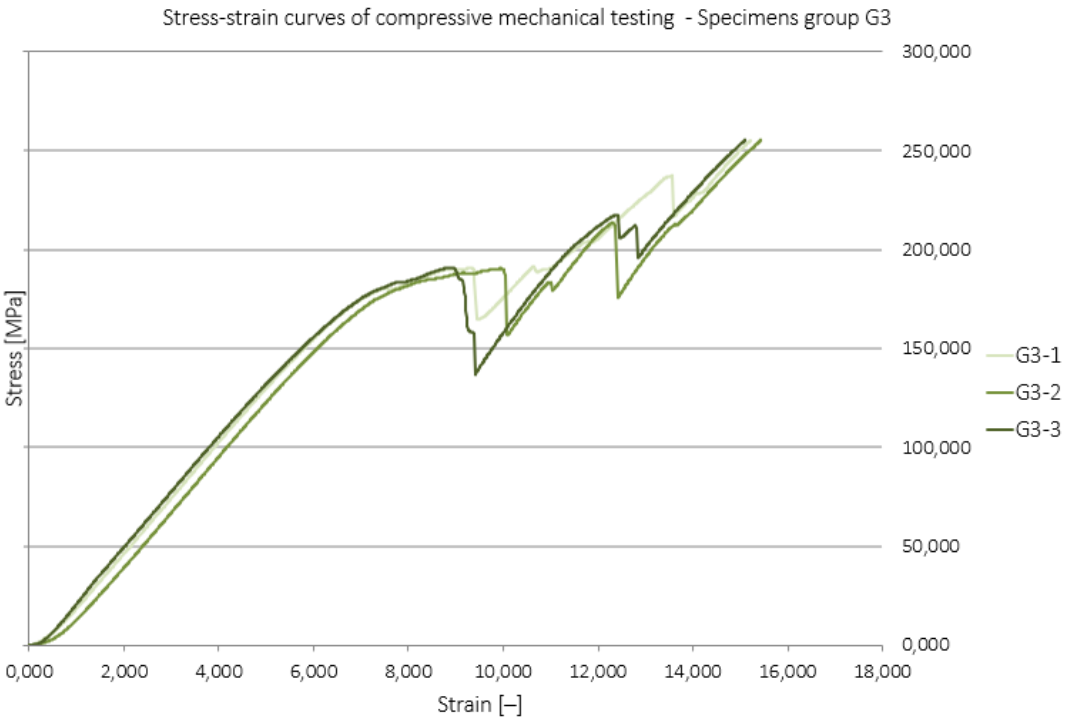
Figure 9.4: Stress-strain curve obtained from compressive testing of gyroids number 3
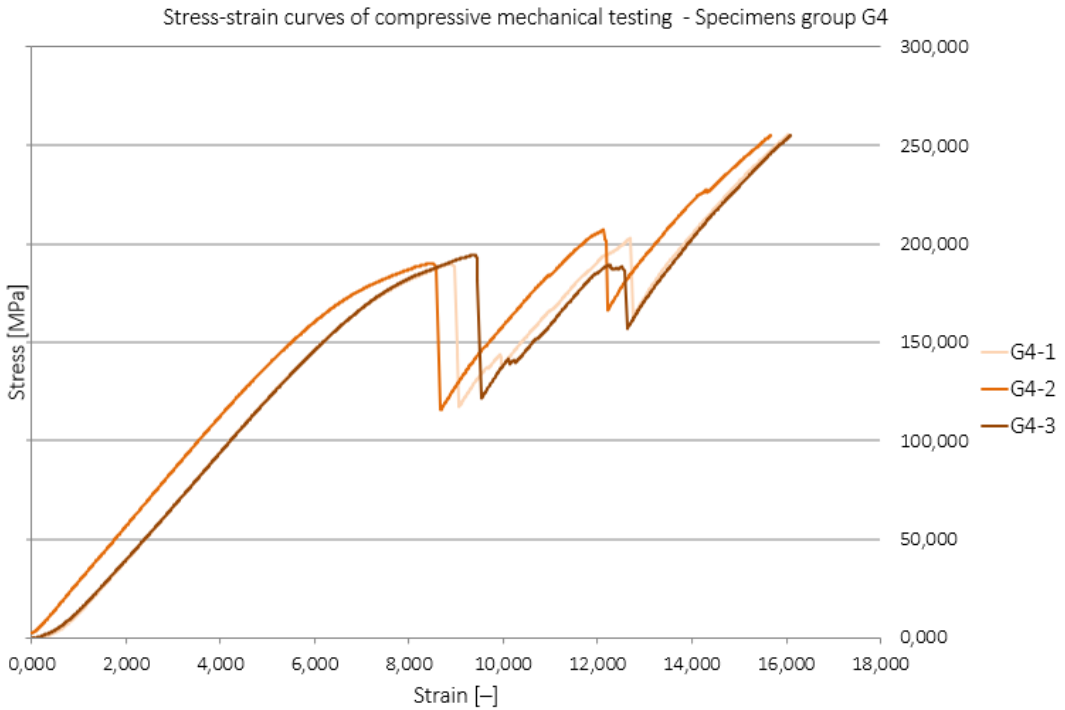
Figure 9.5: Stress-strain curve obtained from compressive testing of gyroids number 4

Based on the stress-strain curves and mechanical properties we can observe specific behavior of structures. As predicted, the elastic modulus varied depending on the porosity of the structures. It is logical that based on the amount of material in the sample while sustaining the same type of morphology, the mechanical properties vary. Basically, the following rule can be applied that the higher the porosity, the lower the modulus, which is attributed to the introduction of porosity in the samples. What is more, the contractual compressive strength and the first maximum compressive strength also related to the mentioned trend, but the differences between the structures are not that significant. In general, we can state that the first maximum compressive strength is around 200 MPa and the contractual compressive strength is 160 MPa.

As we said earlier, the value of elastic modulus is based on the porosity. In the figure 9.6, we can see the relation between these two properties.
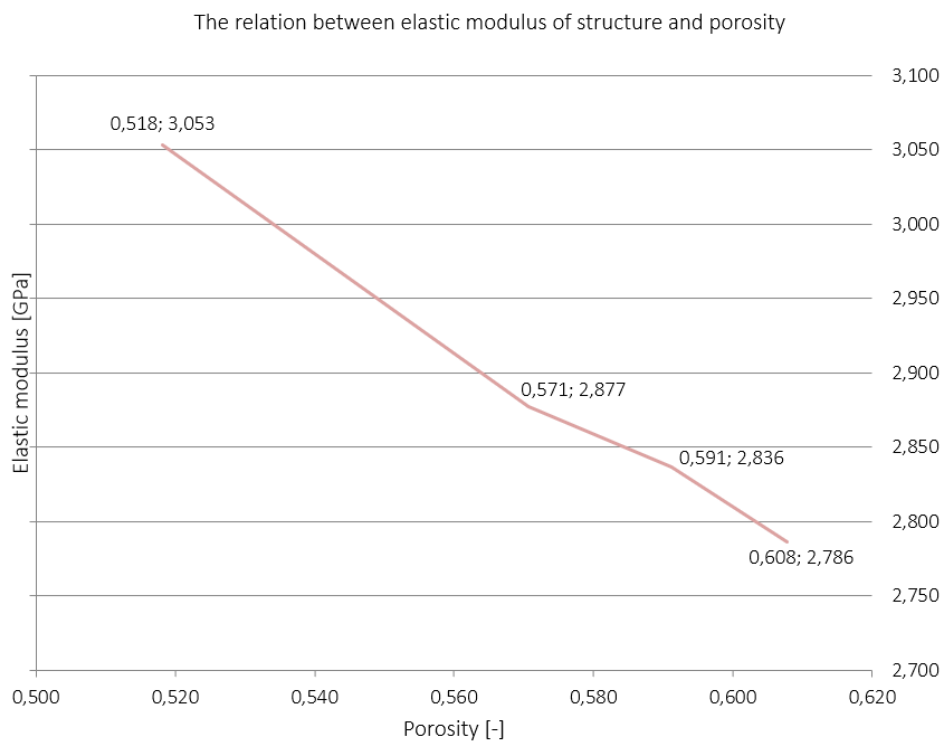
Figure 9.6: The relation between elastic modulus of the gyroid structure and gyroid porosity

9.3 Comparison of gyroid and contemporary structres

The presented paper set goal to improve morphology compared to contemporary trabecular structures. These morphologies were introduced in chapter 8.1. There are Dode Thick, Diamond and Rhombic dodecahedron. This chapter is focusing on the differences in the mechanical properties and the fracture rate in the microscopical level of the structures. In table 9.3, we can see the mechanical properties of structures. As a member of the TAČR project team (project code number TJ01000328), I participated in analytical research of trabecular structure based on Dodethick, Diamond and Rhombic structures. In the following chapter, I would like to compare the mechanical results of these strut-based structures to the gyroid structure.

Table 9.3: Mean values of mechanical properties for each individual gyroid structure

Type of gyroid structure	E	$\sigma_{first,max}$	$\sigma_{0,2}$	n
-	GPa	MPa	MPa	-
Gyroid structure nb 1	3,048	228,501	166,990	0,518
Gyroid structure nb 2	2,868	214,805	161,554	0,571
Gyroid structure nb 3	2,837	190,670	157,764	0,591
Gyroid structure nb 4	2,772	191,434	154,119	0,608
Diamond (0,75 mm)	2,884	88,649	86,647	0,366
Diamond (1,00 mm)	3,508	141,924	126,449	0,376
Dode Thick (1,00 mm)	3,713	N/A	142,218	0,374
Dode Thick (1,25 mm)	2,838	98,211	84,694	0,408
Rhombic dodecahedron (1,25 mm)	3,822	N/A	N/A	0,261
Rhombic dodecahedron (1,00 mm)	2,631	90,201	78,388	0,493

The elastic moduli of contemporary structures are based on porosity. The sensitivity of porosity increasement is, however, significantly higher. A small change in the porosity of diamond morphology can lead to an increment of 0,2 in the value of elastic modulus. The same effect can be seen in the Dode Thick and rhombic dodecahedron morphology. It is important to mention that elastic moduli of the gyroid structures and contemporary structures are close to the elastic modulus of trabecular human bone 2,71-9,1 GPa. We can conclude that the differences in elastic modulus are not a suitable property for comparison of structures.

The first maximum compressive strength and the contractual compressive strength, however, show huge differences across specimens. It is important to mention, that previous tests were executed by using a machine with a lower maximal force of 30 kN. This is the reason, why the strength of Dode Thick (1,00 mm) and Rhombic dodecahedron (1,25 mm)

were not able to obtain. Although some of the values are unknown, we can state that, in general, gyroid structures feature higher strength. This fact is crucial because strength is related to the durability of the implant. For our purposes, the elastic modulus is mainly important in relation to the stress shield effect. On the contrary, the strength is related to the loading which can implant withstand before failure. In the figure 9.7, we can see the stress-strain curves of all structures. For clarity, there were chosen just one strain-stress curve for each gyroid structure. According to the figure, we can see differences in the strength of structures. Strut-based structures have much lower strength than gyroid structure. What is more, there is a difference at the beginning of the curves. If we take a closer look, we can see that gyroid structures are linear from the beginning. On the contrary, the strut-based structure has a non-linear beginning. It is assumed that the huge role of this behavior was due to fractures made by the production of strut-based structure. It took some amount of force until the material "settled."

In conclusion, we can state that the elastic moduli of the gyroid structures and control structures are similar. The main difference is that the gyroid structure has higher compressive strength than contemporary structures. Thus gyroid structure withstands much more loading before failure.
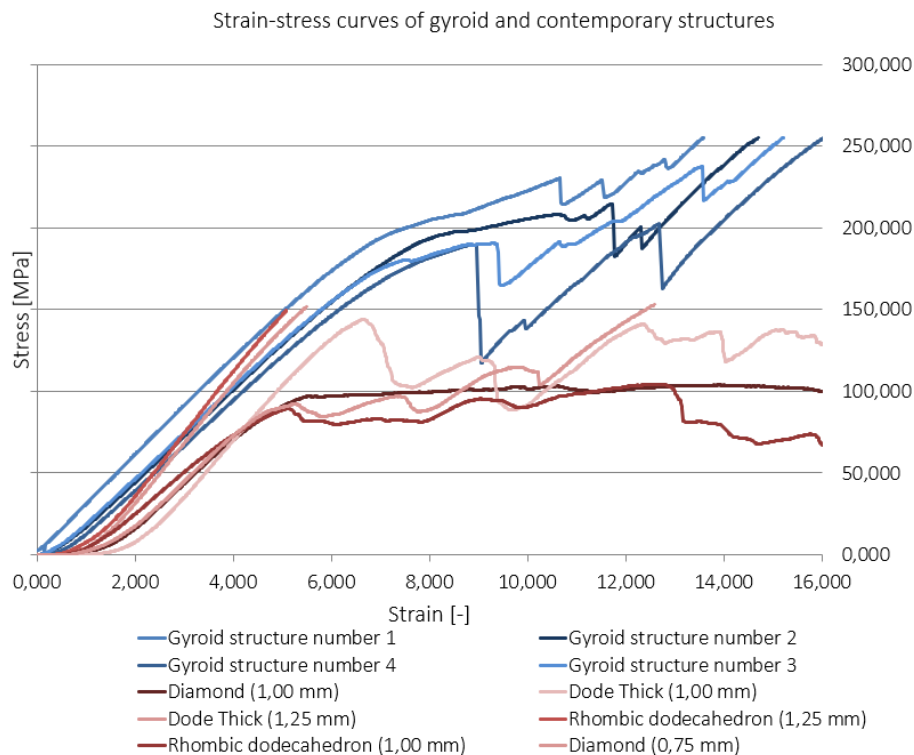
Figure 9.7: The overview of stress-strain curves of gyroid and contemporary structures. We can see similar elastic moduli but significantly different strength.

The fracture rate was introduced in chapter 8.1. There were found fractures in specimens with strut-based morphology. The problem is connected to the production process. During

3D-printing, one layer is placed upon the other. The cooling rates of layers are different, and It causes the fractures in the construction. The main idea behind the solution is to use plane-based morphology in order to deal with these fractures. We can see the difference in the figures 9.8. In conclusion, fractures can split in time and lead to losing the implant.
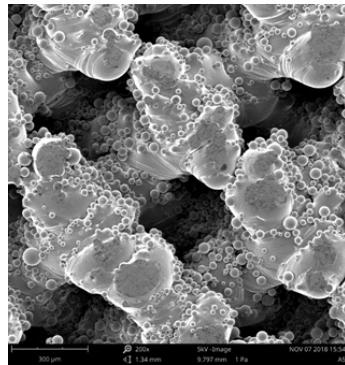
((a)) Microscopical detail of strut-based structure
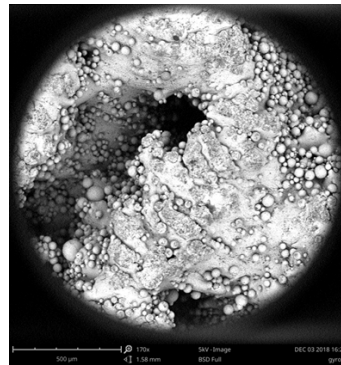
((b)) Microscopical detail of gyroid structure

Figure 9.8: We can see the differences between the amount of microfractures between plane gyroid structure and strut-based structure

For safety reasons, I assume that every possible loading which the implant needs to withstand causes just elastic deformation. For this reason, we consider only a linear stress-strain diagram for modeling which will be described in the next chapter. Even under the condition, the possibility of overloading needs to be consider. In this case, we need the structure to be as compact as possible even after overloading. The comparison of strut-based structure and gyroid structure shows us in the figure 9.9 that the strut-based structure tends to lose parts of the material which can cause necrosis. In contrast, the gyroid structure is compact ever after overloading. The use of plane-based morphology such as gyroid structure can increase the successful rate of implant surgeries.
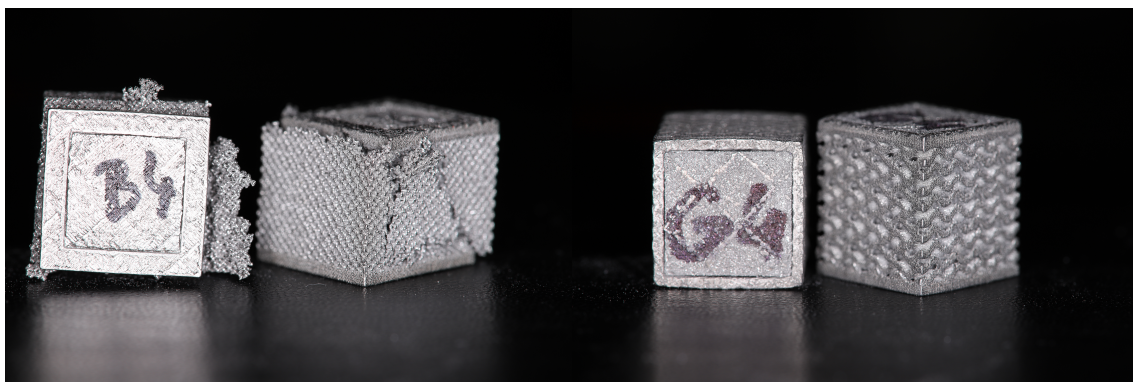
((a)) Overloading of strut-based structure   ((b)) Overloading of gyroid structure

Figure 9.9: Overloading comparison of strut-based structure and gyroid structure

TENTH

NUMERICAL MODEL

10.1 Meshing

The main problem during my thesis was the process of geometrical modeling and meshing of the structure. These two steps were deeply connected because if there is a singularity or a split edge in the geometrical model, then the meshing was problematic. At first, I plotted the gyroid structure in the K3DSurf by using geometrical equation 8.1 and exported it into the .obj file format. Afterward, I utilized the approach used in the study [46] and I imported the plot into the Blender which is open source 3D creation software. It is mainly used for animation, rendering, and video editing. There, I was able to modify the thickness for the needed size and exported it into the .stl format. The next step was the import of the new 3D structure into "Netfabb." It is software by Autodesk company for 3D modeling and printing, where I cut the sides of the gyroid to achieve the cubic shape. The final step was the import into ANSYS. This model, however, was not suitable for numerical analysis because of its defects and short edges. Although The ANSYS software has various tools for model repair, the model was poorly designed, so the meshing was not successful. Thus, a different approach had to be performed.

The next step was to achieve a less problematic geometrical model by using different plotting software and make the way from the geometrical model software to ANSYS software as short as possible. This being said, I made the geometrical model directly in the Netfabb software and modified the thickness of the gyroid structure there.

The essential factor had to be taken into account during the making of the model that the limit of ANSYS academic license is the 512K cells/nodes. Thus, the model accuracy had to be reduced to respect the limits. What is more, the gyroid is not symmetrical structure around any axis, so it was not possible to mirror the mesh and bypass the ANSYS limitation. In consideration of the previous, I was not able to model multi gyroid structure, and the simple gyroid structures models were set to be the goal of the thesis. All multi gyroids were cut in the ANSYS to be a simple gyroid structure. The dimension of specimen

was chosen according the highest dimension of unit cell. According to gyroid structure number 1, the dimension of cutting box was set to 3 mm. All of models were meshed successfully by the automatic meshing method. I had to lower the accuracy of gyroid plotting for structures number 3 and 4 because of the academic license limitation. The meshes can be see in the figure 10.1.
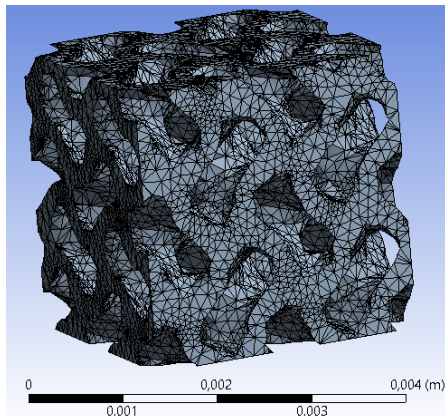
((a)) Gyroid structure number 1 - 118 313 nodes/ 68 708 elements
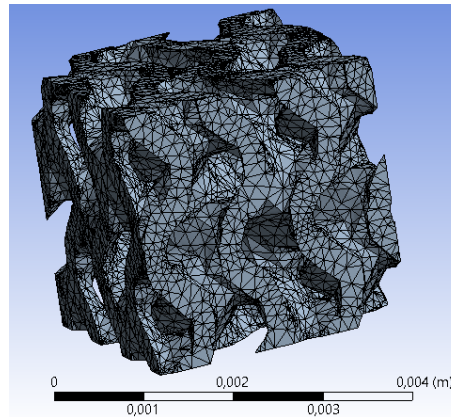
((b)) Gyroid structure number 2 - 119 653 nodes/69 601 elements
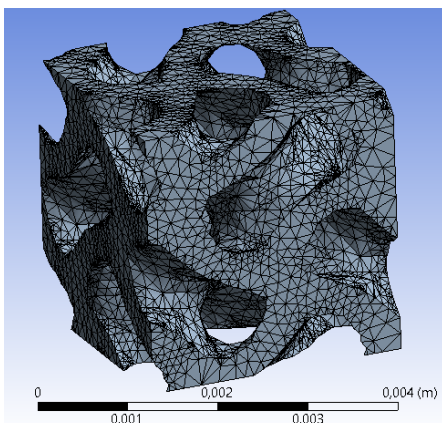
((c)) Gyroid structure number 3 - 119 653 nodes/ 69 601 elements
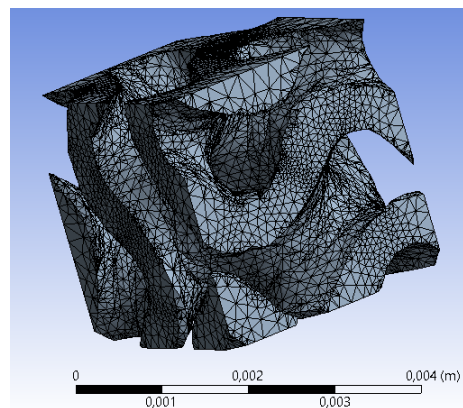
((d)) Gyroid structure number 4 - 218 763 nodes/ 126 647 elements

Figure 10.1: Meshes of gyroid structures

10.2 Load program and analysis settings

The next step of the process was the setting of the loading program. It had to respect the experimental loading of the structures according to the ISO 13314:2011 Mechanical testing of metals – Ductility testing – Compression test for porous and cellular metals which specify a test method for compressive properties of porous and cellular metals with a porosity of 50% or more. This procedure is detailed analyzed in chapter 9.

Therefore, all of the specimens had to be loaded by the remote displacement 1 mm/min. In general, the rigid body has 6 degrees of freedom which I need to constrain. In consonance with the experiment, I fixed all of the degrees on one side of the gyroid structure by fixed support. On the opposite side, I set the loading by remote displacement. The remote displacement loading had rigid behaviour and ramped rotation around all axes in order to represent the experiment as much as possible

((a)) One side of the gyroid is constrained by the fixed support. It is labelled by blue colour

((b)) Yellow colour of the gyroid platform represent the remote displacement loading
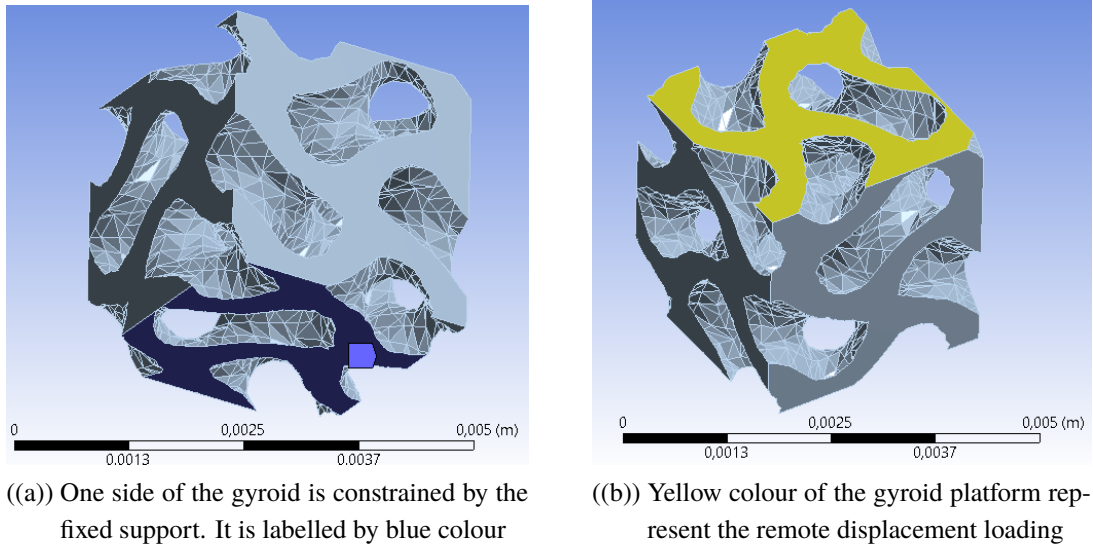
Figure 10.2: The constrains and loading of the gyroid structure

As we said in chapter 9.3, we assume just elastic part of the stress-strain curve because of implant safety reasons. We do not accept the state when there is plastic deformation which can lead to the loss of the implant. During observation of stress-strain curves of gyroid structures in chapter 9.2, I noticed that 150 MPa is the point when all of the gyroid structures start the process of hardening. Naturally, this value of stress is achieved under different forces based on gyroid morphology and different strain.

Let us discuss the computation of model input for one gyroid. First of all, we had to state the force reaction which is caused by remote displacement. We obtained the value of force which caused stress equal to 150 MPa from experiment data:

$$F_{model\ gyroid} = \frac{F_{experimental\ gyroid} * A_{model\ gyroid}}{A_{experimental\ gyroid}}$$

$$F_{model\ gyroid} = \frac{F_{experimental\ gyroid} * 3 * 3}{14 * 14}$$

(10.1)

, where $F_{model\ gyroid}$ stands for force reaction caused by remote displacement, $F_{experimental\ gyroid}$ stands for value of force obtained from experiment which caused stress equal to 150 MPa, $A_{model\ gyroid}$ stands for contact loading area of gyroid which underwent experimental testing, $A_{model\ gyroid}$ stands for contact loading area of gyroid model. The calculated force had to correspond with the force probe on the top of the loaded model.

The next step was to determine the final deformation of model. For our purpouses, a simplification had to be maken that strain is equal throughout the gyroid structure. Afterward, I could compute the require deformation of our model:

$$u_{model\ gyroid} = \frac{u_{experimental\ gyroid} * h_{model\ gyroid}}{h_{experimental\ gyroid}}$$

$$u_{model\ gyroid} = \frac{u_{experimental\ gyroid} * 3}{14}$$

(10.2)

, where $F_{model\ gyroid}$ stands for required remote displacement loading, $F_{experimental\ gyroid}$ stands for value of deformation from experiment which caused stress equal to 150 MPa, $h_{model\ gyroid}$ stands for the height of gyroid which underwent experimental testing, $h_{model\ gyroid}$ stands for the height of the gyroid model.

The previous values were essential for computation. First of all, I set the remote displacement according to equation 10.2 and then I changed the Elastic modulus to achieve the value of force from equation 10.1.

In the table under, we can find the results of approximations. We can see that the elastic modulus of material Ti6Al4V is significantly lower than the value according to the material list 8.2 which is equal to 115 GPa. It is assumed that the reason for such a high difference is due to the problematic loading of samples. In figures 9.9, we can see that producer of gyroid samples placed a selvage on the edge of platforms. It caused that the loading was distributed mainly through outer parts of gyroid structures, whereas the loading of the numerical model was placed on the complete platform. The time-consumption of the production of samples, which was about 2 months, enabled me to repeat experimental testing.

Table 10.1: The model verification

Type of gyroid structure	Force probe	Strain of model	Elastic modulus of material
-	N	%	GPa
Gyroid structure nb 1	1350	5,1	14,57
Gyroid structure nb 2	1350	5,8	12,98
Gyroid structure nb 3	1350	6,1	12,2
Gyroid structure nb 4	1350	6,25	11,11

In figures 10.3 and 10.4, we can see the deformation and total stress distribution of the stiffest model number 1 with the unit cell dimension 1,4 mm. In following figures 10.5, 10.6, 10.7 and 10.8, we can see the stress-strain curve obtained from experiment testing and the model curve-fitting solution:
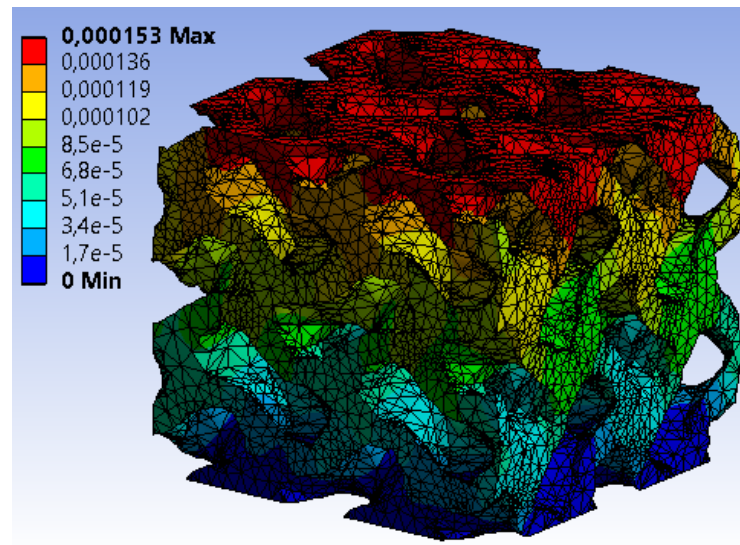
Figure 10.3: The deformation of gyroid structure in meters
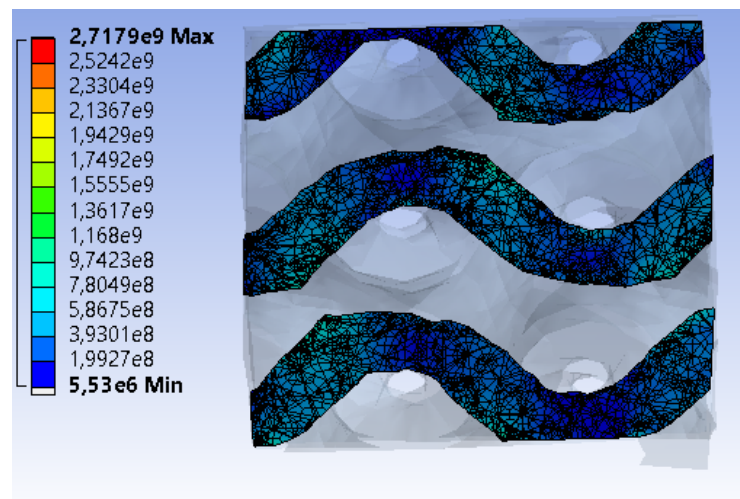
Figure 10.4: In the figure, we can see a cross-section of equivalent stress in Pa. We can see singularities in the edges of the cross section. In multi-gyroid structure, these singularities do not exist. They are product of the simplyfication of the whole gyroid structure. After cutting of the multi gyroid structure, there were created sharp edges. In the loading process, these are the places where maximum stress is shown.
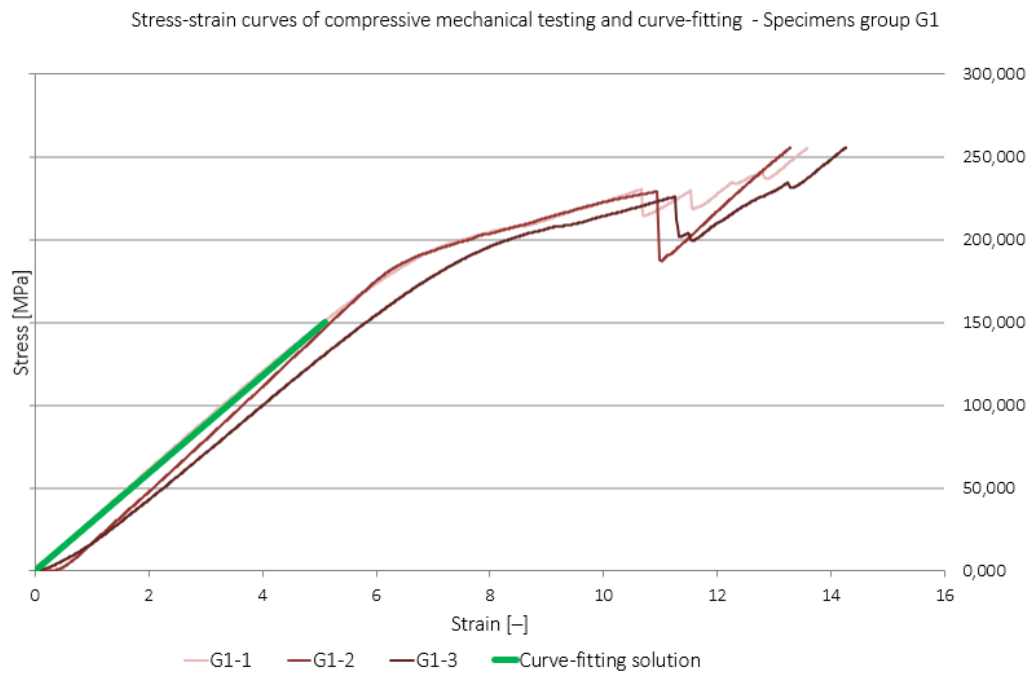
Figure 10.5: Stress-strain curve obtained from compressive testing and model curve-fitting of gyroid number 1
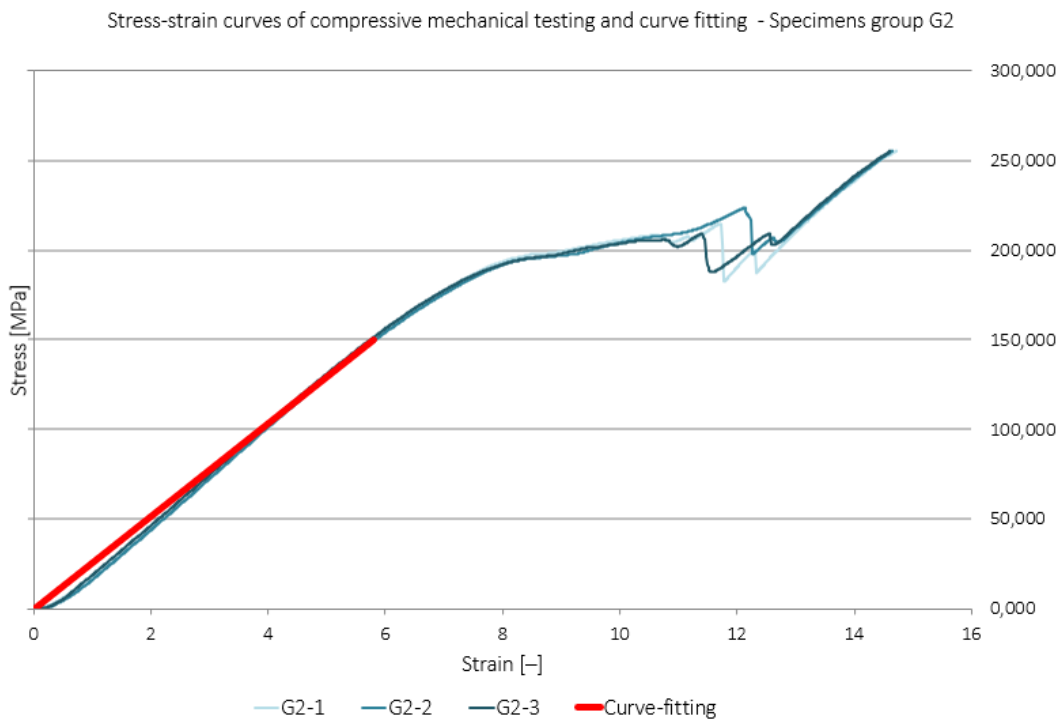
Figure 10.6: Stress-strain curve obtained from compressive testing and model curve-fitting of gyroids number 2
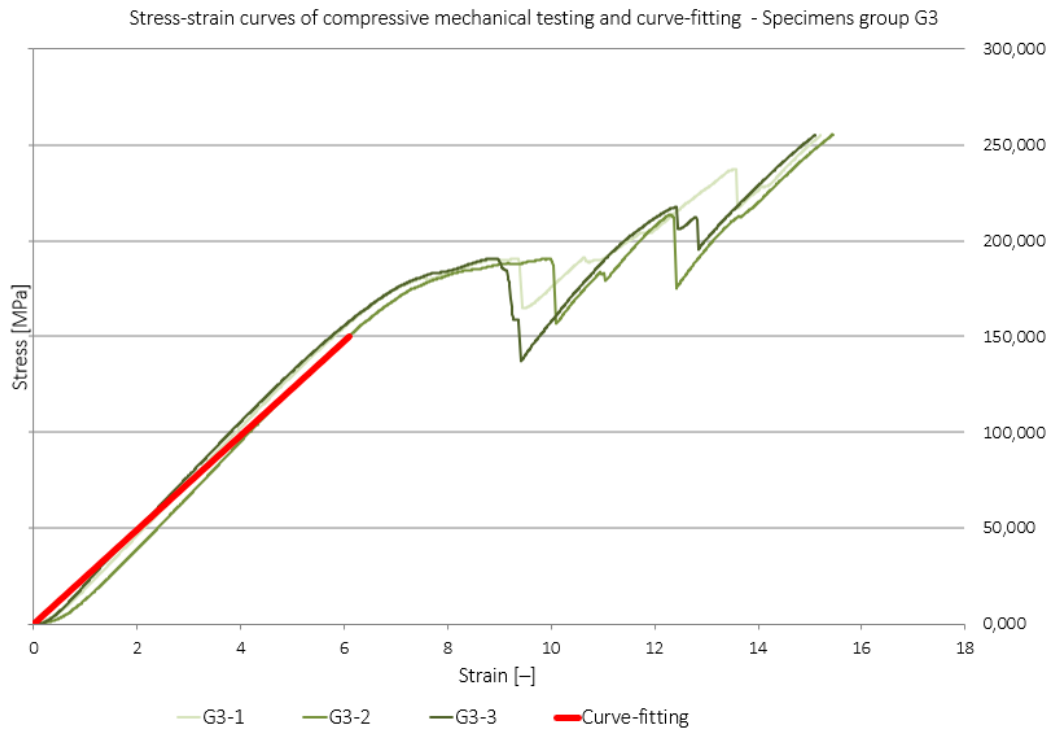
Figure 10.7: Stress-strain curve obtained from compressive testing and model curve fitting of gyroids number 3
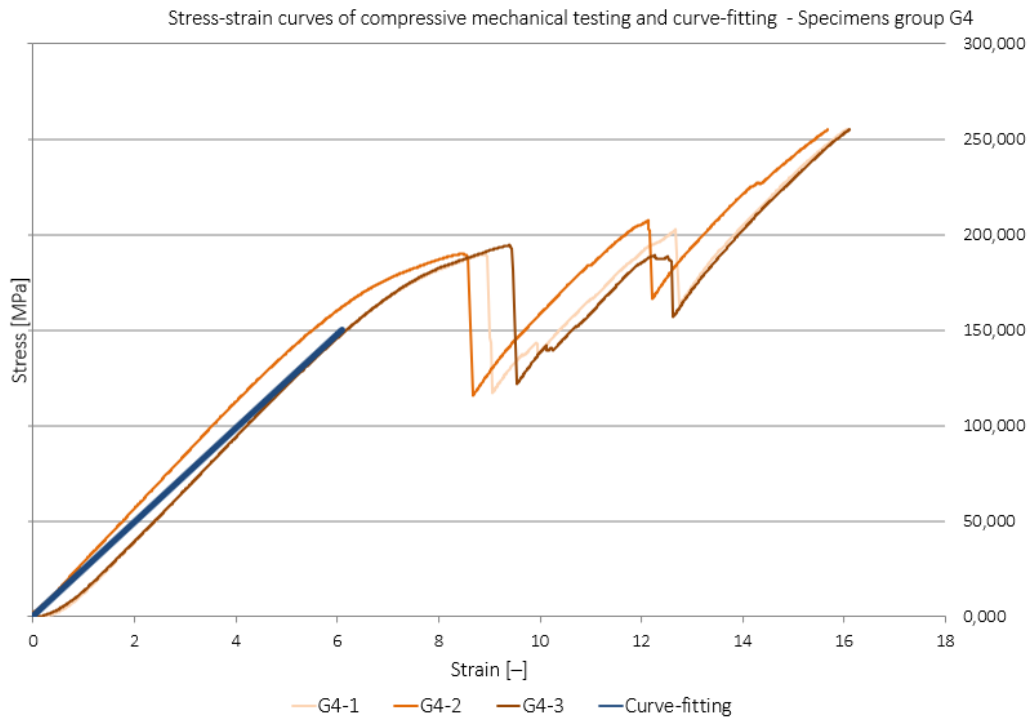
Figure 10.8: Stress-strain curve obtained from compressive testing and model curve fitting of gyroids number 4

10.3 Future prospects

The main objective of the presented paper deals with a brief analysis of trabecular structure as a substitution for surface modification of implants. Although, the durability of implants depends on various factors such as implant construction, application and healing process, the presented paper focus only on the construction part. Moreover, the thesis deals just with three parts of problems which are 3D printing problems, pore size, and stress shield effect. The solving of all problems connected to implant construction is beyond the limits of the thesis.

Problems connected to production are listed in the chapter 8.1. Two types of fractures can occur in the 3D printed product. The first part of fractures can be found in the border area of a homogenous and trabecular part in the figure 8.3 due to different cooling velocities of parts. These fractures can be minimalized by reducing the mass of the homogenous part of the structure. There are two types of solutions. The first solution deals with the problem by placing pores in the solid part. In the other solution, the implant could consist of 2 different trabecular parts: the outer part and the inner part. The outer part contains a large dimension of unit cell resolution of trabecular structure suits to contact with living tissue. The inner part disposes small dimension of the unit cell in order to achieve high Young modulus and to be sufficient support for the artificial tooth. This type of gradient porosity can make full use of 3D printing possibility. The solution of the second part of fractures was introduced in the chapter 9.3. If the strut-based morphology is substitute with plane-based morphology, the fracture rate is prone to be minimal. We can see the result in figure 9.8. The solutions mentioned above can increase the probability of successful implant surgery.

Pore optimilization was done according to study led by Taniguchi[20]. The pore size of bone ingrowth was set to be optimal if it is in range of 450-750μm. This criterium was fullfilled by gyroid structures number 2 and 3. For the futher research, it is recommended to undergo in-vivo test for gyroid structures which can determinate if the osseointegration is succesful.

The next problem called the stress shield effect is detailly described in chapter 3.1. The effect can be reduced by using a porous structure such as gyroid. The global elastic modulus needs to be close to the elastic modulus of trabecular bone in order not to create a stress shield. The effect can lead to resorption of bone or loss of the implant. The range of elastic modulus of trabecular bone is 2,71-9,1 GPa. [8]. All gyroid structures fulfilled the criterium. It is essential to mention that the range is quite vast because of the variety of conditions that relate to the age, diseases, and lifestyle of surveyed. There lies another advantage of porous structures. There can be modified to be custom-made to be suitable for a specific patient. The variability of modification is, however, limited because of the minimum pore size for bone ingrowth. I assumed just linear part of stress-strain curve. Simlification was made because of safety reason. Even under the condition, the

possibility of overloading needs to be consider. In this case, we need the structure to be as compact as possible even after overloading. In figure 9.9, we can see that gyroid structure is compact even after overloading in compared to strut-based structure.

The following research should aim to model the whole gyroid structure which could represent the structure behavior more accurately. I was not able to develop a more complex model because of ANSYS license limitation. Even if I were able to obtain a full license, the next problem would be the computing power of my personal computer. Multi gyroid model could determine the global elastic of the structure precisely. The next step would be the substitution of gyroid by a homogenous structure with similar mechanical properties. This could allow us to model the whole implant with reasonable computing power. In figures 10.9, we can see the possible future of dental implants with gyroid structure instead of surface modification in the contact area with living tissue. It is essential to continue with the research to face other problems that can occur through processes of implementation.
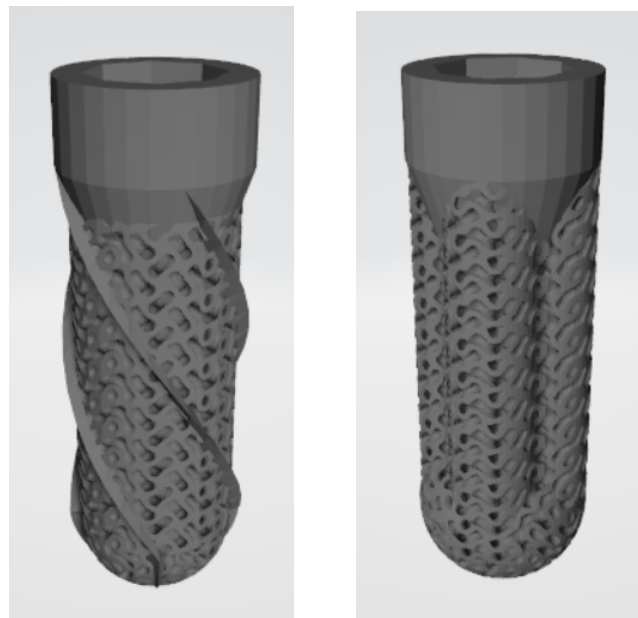
((a)) Push-in implant with helix stabilization

((b)) four-leaf push-in implant

Figure 10.9: The possible future of dental implants

ELEVENTH

CONCLUSION

The goal of the presented paper was set to design efficient trabecular structure which can be used for a variety types of implants in the barrier between bone and artificial material. It can substitute contemporary surface modifications to avoid the stress shield effect and maximalize the bone ingrowth. In order to, achieve the goal of the thesis, It was set to determinate the most suitable structure and design the model in the FEM software ANSYS. Afterward, the specimen would have been produced by using 3D printing technology, which is the method used for the creation of complex structures. The material was selected Ti6Al4V. It has a rich history of using in bioengineering as a biomaterial. What is more, it is suitable in the form of powder as input material in 3D printing. In the end, the specimen would have undergone mechanical testing, and the model would have been verified.

At first, there were printed strut-based structures with a platform on two opposite sides which showed two types of discontinuities. These fractures can split in time and lead to necrosis or aseptic loosing of the implant. The first group of fractures was between the homogenous part and the trabecular part, which can we see in figure 8.3(a) and 8.3(b) due to different cooling velocities between homogenous part and trabecular part during the printing process. The problem was solved by reducing the platform mass. We can see the process in figure 8.4. The second group of fractures was found inside the trabecular structure. Based on previous, it was supposed that the strut-based structure is not suitable as the porous part of the implant and the plane structure is more convenient for the trabecular part. In conclusion, the gyroid structure was selected. There were modelled four types of multigyroid structure with the different dimension of unit cell. Multi gyroid structures were chosen to respect the behavior of the structure as high as possible.

The mechanical experiment of the gyroid structures was undergone according to international standard ISO 133114:2011 Mechanical testing of materials - Ductility testing-Compression test for porous and cellular metals. Although, the standard is intended for porous and foam metals with porosity higher than 50% and all of the gyroid structures satisfy the criterium. There were made compressive tests so that the numerical verification

of the models can have been taken. The machine MTS Alliance RT-30 was used for compressive testing. There were examined the most important factors such as global elastic moduli, the first maximum compressive strength, contractual compressive, and porosity. The results of mechanical testing were made for each gyroid structure and compared with the contemporary strut-based structures. After evaluation, there was observed that elastic modulus of gyroid and strut-based structure are close to the elastic modulus of human trabecular bone. In comparison, while maintaining a similar Elastic modulus, the difference in strength was significant. We can see the stress-strain curve of structure in figure 9.7. At the end of the mechanical experiment part, there is discussed the rate of fractures of plane-based and strut-based structure. In summary, It can be stated that the probability of fracture is significantly higher during the production of the strut-based structure.

The following part of the thesis deals with the structural analysis of the gyroid structure. During the meshing, few limiting factors influenced the modeling such as academic license limitation and the communication between software. The second mentioned refers to the process of developing the geometrical model. The process needed to be controlled in order not to damage the model data by exporting into an invalid state for the other software. Based on limiting factors, the goal of the thesis was set to model single gyroid structures. For safety reason, there was consider only linear part of the stress-strain diagram. The mechanical properties were verified based on mechanical experiments by using the curve-fitting method. That, concretely, was done by modifying the elastic modulus of the material. The final elastic modulus of material was significantly lower than the one according to the material list 8.2. It is assumed that the reason lies in the fact that producer of gyroid samples placed a ledge on the platform edge. We can see it in the figure 9.9. It caused that load of gyroid structure were not distributed throughout whole structure but just on the edges. On contrary, the load of numerical model was placed on the whole platform. It resulted in difference between numerical model and experimental results. For following reaseach is esssential to repeat experiment with corrected gyroid structures in collaboration with the producer of gyroid structures company "ProSpon spol. s r.o." In the end, there is discussed the possibility of future research.

LIST OF FIGURES

LIST OF TABLES

BIBLIOGRAPHY

[1] T. Vieru. Mathematics links structure to function in leaves, [online] Available at:. https://news.softpedia.com/news/Mathematics-Links-Structure-to-Function-in-Leaves-269372.shtml. [Accessed: 5.4.2019].

[2] A. Kitabjian. Trabecular bone morphology changes may predict bone strength in girls [online] Available at:. https://www.endocrinologyadvisor.com/home/topics/pediatric-endocrinology/trabecular-bone-morphology-changes-may-predict-bone-strength-in-girls/. [Accessed: 5.4.2019].

[3] M. M. Barak, M. A. Black. A novel use of 3d printing model demonstrates the effects of deteriorated trabecular bone structure on bone stiffness and strength. *Journal of the Mechanical Behavior of Biomedical Materials* **78**:455–464, 2018. DOI:10.1016/j.jmbbm.2017.12.010.

[4] F. Härle, M. Champy, B. Terry. *Atlas of Craniomaxillofacial Osteosynthesis: Microplates, Miniplates,and Screws*. Thieme, 2nd edn., 2009.

[5] M. Mostakhdemin. Mechanical behavior of trabecular bone. *Trauma Plating Systems* pp. 33–41, 2017. DOI:10.1016/B978-0-12-804634-0.00003-3.

[6] Current knowledge in trabecular bone score – TBS® should be carefully used, [online] Available at:. https://quibim.com/2016/05/31/current-knowledge-in-trabecular-bone-score-tbs-should-be-carefully-used/. [Accessed: 18.3.2019].

[7] A. Vainionpää. *Bone adaptation to impact loading - significance of loading intensity*. Oulu university press, Oulu, 2007.

[8] D. Wu, P. Isaksson, S. J. Ferguson, C. Persson. Young's modulus of trabecular bone at the tissue level. *Acta Biomaterialia* **78**:1–12, 2018. DOI:10.1016/j.actbio.2018.08.001.

[9] C. Schwartz-Dabney, P. Dechow. Variations in cortical material properties throughout the human dentate mandible. *American Journal of Physical Anthropology* **120**(3):252–277, 2003. DOI:10.1002/ajpa.10121.

[10] K. Verplancke, W. D. Waele, H. D. Bruyn. Dental implants, what should be known before starting an in vitro study, 2011.

[11] S. Liu, Y. C. Shin. Additive manufacturing of ti6al4v alloy **164**, 2019. DOI:10.1016/j.matdes.2018.107552.

[12] Z. J. Wally, A. M. Haque, A. Feteira, et al. Selective laser melting processed ti6al4v lattices with graded porosities for dental applications. *Journal of the Mechanical Behavior of Biomedical Materials* **90**:20–29, 2019. DOI:10.1016/j.jmbbm.2018.08.047.

[13] M. Leary. Surface roughness optimisation for selective laser melting (slm). *Laser Additive Manufacturing* pp. 99–118, 2017. DOI:10.1016/B978-0-08-100433-3.00004-X.

[14] M. Ridzwan, S. Shuib, A. Hassan, et al. Problem of stress shielding and improvement to the hip implant designs. *Journal of Medical Sciences(Faisalabad)* **7**(3):460–467, 2007-3-1. DOI:10.3923/jms.2007.460.467.

[15] S. Leuders, M. Thöne, A. Riemer, et al. On the mechanical behaviour of titanium alloy tial6v4 manufactured by selective laser melting. *International Journal of Fatigue* **48**:300–307, 2013. DOI:10.1016/j.ijfatigue.2012.11.011.

[16] G. Kasperovich, J. Hausmann. Improvement of fatigue resistance and ductility of tial6v4 processed by selective laser melting. *Journal of Materials Processing Technology* **220**:202–214, 2015. DOI:10.1016/j.jmatprotec.2015.01.025.

[17] C. R. Bragdon, M. Jasty, M. Greene, et al. Biologic fixation of total hip implants **86**:105–117, 2004. DOI:10.2106/00004623-200412002-00015.

[18] C. M. Murphy, M. G. Haugh, F. J. O'Brien. The effect of mean pore size on cell attachment, proliferation and migration in collagen–glycosaminoglycan scaffolds for bone tissue engineering. *Biomaterials* **31**(3):461–466, 2010. DOI:10.1016/j.biomaterials.2009.09.063.

[19] H. Wang, K. Su, L. Su, et al. The effect of 3d-printed ti6al4v scaffolds with various macropore structures on osteointegration and osteogenesis. *Journal of the Mechanical Behavior of Biomedical Materials* **88**:488–496, 2018. DOI:10.1016/j.jmbbm.2018.08.049.

[20] N. Taniguchi, S. Fujibayashi, M. Takemoto, et al. Effect of pore size on bone ingrowth into porous titanium implants fabricated by additive manufacturing. *Materials Science and Engineering: C* **59**:690–701, 2016. DOI:10.1016/j.msec.2015.10.069.

[21] V. dos Santos, R. N. Brandalise, M. Savaris. *Engineering of biomaterials*. Springer Berlin Heidelberg, New York, NY, 2017.

[22] A. Šimůnek. *Dentální implantologie*. ARTILIS, Hradec Králové, 3rd edn., 2017.

[23] H. S. Alghamdi, J. J. van den Beucken, J. A. Jansen. Osteoporosis – fracture healing and osseointegration. *Drug Discovery Today: Disease Models* **13**:3–9, 2014. DOI:10.1016/j.ddmod.2014.10.001.

[24] J. Park, M. Ye, K. Park. Biodegradable polymers for microencapsulation of drugs. *Molecules* **10**(1):146–161, 2005. DOI:10.3390/10010146.

[25] Q. Ran, W. Yang, Y. Hu, et al. Osteogenesis of 3d printed porous ti6al4v implants with different pore sizes. *Journal of the Mechanical Behavior of Biomedical Materials* **84**:1–11, 2018. DOI:10.1016/j.jmbbm.2018.04.010.

[26] T. Ahmed, H. Rack. Phase transformations during cooling in titanium alloys. *Materials Science and Engineering: A* **243**(1-2):206–211, 1998. DOI:10.1016/S0921-5093(97)00802-2.

[27] P. Dungl. *Ortopedie*. Grada, Prague, 2nd edn., 2014.

[28] The hip, [online] Available at:. http://bjdonline.org/the-hip//. [Accessed: 30.3.2019].

[29] Hip Joint Replacement Surgery, [online] Available at:. https://www.healthpages.org/surgical-care/hip-joint-replacement-surgery/. [Accessed: 29.3.2019].

[30] Birmingham hip Resurfacing System, [online], Available at:. https://www.verywellhealth.com/birmingham-hip-resurfacing-system-189866/. [Accessed: 19.3.2019].

[31] Two types of hip implants, [online] Available at:. https://www.mayoclinic.org/tests-procedures/hip-replacement/multimedia/two-types-of-hip-implants/img-20007253.

[32] What is a patellar tendon tear?, [online] Available at:. https://www.jeffreybergmd.com/what-is-a-patellar-tendon-tear-video/. [Accessed: 18.3.2019].

[33] Joint replacement, [online] Available at:. http://www.museumofhealthcare.ca/explore/exhibits/joints/knee-replacement.html. [Accessed: 16.3.2019].

[34] H. S. Selhi. Knee replacement [online], Available at:. http://drharpalsingh.com/knee-replacement.php. [Accessed: 28.3.2019].

[35] Biomaterials in dental implants / dental implant courses by indian dental academy [online] Available at:. https://www.slideshare.net/indiandentalacademy/9biomaterials-in-dental-implants-dental-implant-courses-by-indian-dental-academy. [Accessed: 24.3.2019].

[36] Overview of Formiggini endosseous implant design, [online], Available at:. http://www.linkowlibrary.org/dental-book/3101/Overview-of-Formiggini-s-endosseous-implant-design/. [Accessed: 24.3.2019].

[37] An overview of subperiosteal implantation [online], Available at:. http://www.linkowlibrary.org/dental-book/3079/An-overview-of-subperiosteal-implantation. [Accessed: 24.3.2019].

[38] Branemark System Zygoma - procedure manual, [online], Available at:. https://www.nobelbiocare.com/international/en/home/products-and-solutions/library/manuals.html. [Accessed: 24.3.2019].

[39] S.-H. M. et.al. The effect of implant shape and bone preparation on primary stability **40**, 2010. DOI:10.5051/jpis.2010.40.5.239.

[40] H.-S. Han. Design of new root-form endosseous dental implant and evaluation of fatigue strength using finite element analysis 2009. DOI:10.17077/etd.3rodr4hx.

[41] Zygomatic implants [online], Available at:. https://www.for.org/en/treat/treatment-guidelines/edentulous/treatment-procedures/surgical/surgical-protocols-maxilla/zygomatic-implants. [Accessed: 23.3.2019].

[42] RMO Dual-Top Temporary Anchorage Device from Rocky Mountain Orthodontics, [online], Available at:. https://www.dentalcompare.com/4575-Orthodontic-Micro-Screw-Implant-Anchorage/37534-RMO-Dual-Top/. [Accessed: 20.3.2019].

[43] Titanium alloy (powder) according to EN ISO 9693/DIN EN ISO 22674 type 4, [online] Available at:. https://www.concept-laser.de/fileadmin//user-upload/Datasheet-rematitan-CL.pdf.

[44] J. A. Dolan, M. Saba, R. Dehmel, et al. Gyroid optical metamaterials. *ACS Photonics* **3**(10):1888–1896, 2016-09-22. DOI:10.1021/acsphotonics.6b00400.

[45] J. A. Dolan, B. D. Wilts, S. Vignolini, et al. Optical properties of gyroid structured materials. *Advanced Optical Materials* **3**(1):12–32, 2015. DOI:10.1002/adom.201400333.

[46] L. Germain, C. A. Fuentes, A. W. van Vuure, et al. 3d-printed biodegradable gyroid scaffolds for tissue engineering applications **151**:113–122, 2018. DOI:10.1016/j.matdes.2018.04.037.